

Is the resonant wave interaction approximation consistent with the dynamics of internal wave fields?

Golan Bel¹ and Eli Tziperman²

¹Department of Solar Energy and Environmental Physics, Blaustein Institutes for Desert Research, Ben-Gurion University of the Negev, Sede Boqer Campus 8499000, Israel;
Physics Department, Ben-Gurion University of the Negev, Beer-Sheva 8410501, Israel

²Department of Earth and Planetary Sciences and School of Engineering and Applied Sciences, Harvard University, Cambridge, MA, USA

December 4, 2023

Abstract

Nonlinear interaction and breaking of internal ocean waves are responsible for much of the interior ocean mixing, affecting ocean carbon storage and the global overturning circulation. These interactions are also believed to dictate the observed Garrett-Munk wave energy spectrum, which is still unexplained after 50 years of studies. According to the resonant wave interaction approximation, used to derive the kinetic equation for the energy spectrum, the dominant interactions are between wave triads whose wavevectors satisfy $\mathbf{k} = \mathbf{p} + \mathbf{q}$, and whose frequencies satisfy $\omega_{\mathbf{k}} = |\omega_{\mathbf{p}} \pm \omega_{\mathbf{q}}|$. In order to test the validity of the resonant wave interaction approximation, we examine several analytical derivations of the theory. The assumptions underlying each derivation are tested using idealized direct 2d numerical simulations, representing near-observed energy levels of the oceanic internal wave field. We show that the assumptions underlying the derivations are not consistent with the simulated dynamics. In addition, most of the triads satisfying the resonant conditions do not contribute significantly to nonlinear wave energy transfer in our simulations, while some interactions that are dominant in nonlinear energy transfers do not satisfy the resonance conditions. We also point to possible self-consistency issues with some derivations found in the literature.

1 Introduction

The resonant wave interaction approximation (RWIA) is used to simplify the study of nonlinearly interacting waves (e.g., Phillips, 1981; Davis and Acrivos, 1967). The approximation restricts interactions to wave triads (or quartets when triad interaction is not possible) that satisfy a condition on the wave frequencies of the form $\omega_{\mathbf{k}} = |\omega_{\mathbf{p}} \pm \omega_{\mathbf{q}}|$, in addition to the condition on the wavevectors $\mathbf{k} = \mathbf{p} + \mathbf{q}$. The wave triads that satisfy both conditions form “resonance curves” in wavenumber space on which the significant interaction and energy transfer between wave vectors occur according to the theory. RWIA is used as part of the derivation of the kinetic equation of the weak wave turbulence formalism that aims to simplify the full nonlinear dynamics of weakly interacting wave fields (Hasselmann, 1962; Zakharov, 1965; Zakharov et al., 2012; Nazarenko, 2011).

The RWIA-based weak wave turbulence formalism has been applied to surface ocean waves (Hasselmann, 1962), acoustic waves (L’vov et al., 1997), internal waves in the ocean and atmosphere (McComas and Bretherton, 1977; Müller et al., 1986; L’vov et al., 2012, 2004), and the study of Rossby-gravity wave interactions (Eden et al., 2019a), and has been studied experimentally (Herbert et al., 2010). The weak wave turbulence formalism derives the closed kinetic equation for the energy spectrum. The resulting reduction in the number of interactions also leads to a more efficient computational treatment of the problem.

Our interest here is in the application of RWIA to the problem of a field of interacting internal waves in a stratified fluid. Specifically, in the context of internal ocean waves, the observed internal wave spectrum has been shown to have some universal properties represented by the Garrett-Munk (GM) empirical fit (Garrett and Munk, 1972, 1975; Cairns and Williams, 1976; Garrett and Munk, 1979; Levine, 2002; Le-Boyer and Alford, 2021), which was also studied in numerical simulations (Pan et al., 2020; Chen et al., 2019) although deviations from the GM spectrum were observed (Wunsch and Webb, 1979; Polzin and Lvov, 2011; Pollmann, 2020). This spectrum is not fully understood despite decades of research. Nonlinear internal wave interactions and the resulting energy transfers and wave breaking are responsible for much of the mixing in the ocean interior (Munk and Wunsch, 1998). This mixing plays an important role in the absorption of CO_2 (Sabine et al., 2004), in forcing the large-scale meridional circulation, and consequently in the global meridional ocean heat transport (Bryan, 1987; Nikurashin and Ferrari, 2013). The mixing occurs on scales smaller than can be represented in climate models. Its parameterization requires an understanding of the nonlinear wave interactions, which the RWIA and the accompanying weak wave turbulence formalism aspire to provide.

The key assumption of the RWIA is that the wave amplitudes vary over a timescale longer than the corresponding wave periods. Different derivations of the RWIA approach this condition differently and, therefore, result in different slowness criteria. To study the self-consistency of the RWIA, one can initialize the RWIA-based kinetic equation for the internal wave field spectra with the observed GM spectrum and examine the timescale of the response. It has been found that this (Boltzmann) timescale, is not consistent with the slowness assumption, posing a significant challenge to the theory (Holloway, 1980; L’vov et al., 2012). Taking into account near resonance interactions (L’vov et al., 1997) was suggested to result in a slower and, therefore, self-consistent spectral adjustment timescale (L’vov et al., 2012). The ensemble-averaged rates of energy transfer due to wave-wave interaction in short unforced direct numerical simulations and using the kinetic equation were compared by Eden et al. (2019b, 2020) and found similar. However, the question of the consistency of the kinetic equation and the assumptions used to derive it with the actual dynamics of typical oceanic internal wave fields, as opposed to the self-consistency of the kinetic equation, is still open.

In a recent work, Savva et al. (2021) developed a linear kinetic equation for describing the scattering of internal waves by an assumed unchanging quasi-geostrophic flow. They find that the scattering leads to a cascade to small scales along surfaces of constant frequency in wavenumber space. The cascade results in an internal wave spectrum of k^{-2} for scales smaller than the scale of the internal wave forcing, a cascade that develops without nonlinear wave-wave transfers. This spectrum is similar to the spectra observed in the atmosphere and ocean, suggesting an alternative to the shaping of the spectrum by wave-wave interaction, which is our focus here. Savva et al. (2021) describe the mechanism of interaction in the (WKBJ) limit, where internal wave wavelengths are smaller than QG scales, also analyzed by Kafiabad et al. (2019), as a version of the induced diffusion mechanism of McComas and Bretherton (1977), with the small-K geostrophic mode playing the role of the low-frequency internal wave. They similarly identify the interaction of similar upward and downward propagating waves via scattering with the QG field as the elastic scattering mechanism of McComas and Bretherton (1977). Dong et al. (2020) used the WKBJ approximation yet allowed for slow time-variation of the QG flow and found that internal wave energy can spread both along and across constant frequency surfaces, although Cox et al. (2022) find the results based on stationary QG flows to still be robust for internal waves in 3d. While the scattering of internal waves by a stationary or slowly-varying QG flow may be a very efficient mechanism for cross-scale interactions, the fact that the resulting interactions are interpreted using terms that were derived based on the RWIA suggests that it is still worthwhile going back to this approximation and investigating its validity, as we do here. In addition, the separation of simulated or measured flow into internal waves and QG flow is not uniquely defined if the amplitudes of the internal waves are not very slowly varying, as we find below.

We follow three different derivations of the constraint on the frequencies of interacting waves represented by the RWIA that have been used as part of the weak wave turbulence formalism. Using direct numerical simulations (DNS) of a 2d internal wave field, forced at low wavenumbers and run to a statistical steady state (Appendix A), we test the specific assumptions in each derivation that lead to the above constraint on the frequencies. We also use the DNS, performed with the `flow_solve` model (Winters et al., 2004), to

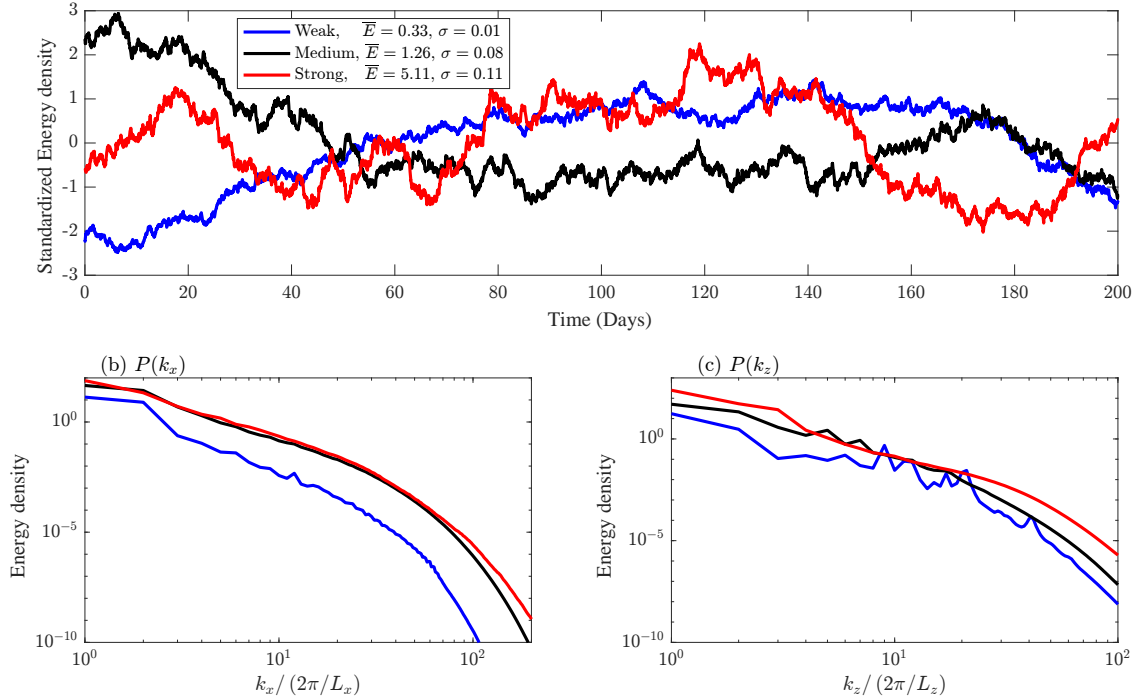


Figure 1: Characterizing the energy in the direct numerical simulations: (a) Time series of standardized total energy per unit volume (J/m^3) for 200 days for the three runs. Energy spectra as a function of the horizontal wavenumber, $P(k_x)$, are depicted in panel (b), and energy spectra as a function of the vertical wavenumber, $P(k_z)$, are depicted in panel (c).

examine all nonlinear interactions in wavenumber space. We find that the dominant interactions are not necessarily on the resonance curves. That is, the nonlinear interaction term calculated from the DNS shows that many of the resonant interactions do not contribute significantly to energy transfers, while there are important interactions that are non-resonant.

Figure 1 shows the time series of the total energy density and vertical and horizontal wavenumber energy spectra. The averaged energy levels of weakly, medium, and strongly forced model runs are 0.33, 1.26, and 5.11 J/m^3 , respectively. The corresponding standard deviations (STDs) of the energy time series are 0.01, 0.08, and 0.11 J/m^3 . Typical energy levels of ocean internal waves were estimated by Levine (2002) as $0.85N/N_{\text{ref}} \text{ J/m}^3$, where $N_{\text{ref}} = 3 \text{ cph}$. We use $N = 2 \text{ cph}$, and this implies an expected energy of 0.6 J/m^3 , somewhere between the results of our simulations with weak and medium forcing amplitudes. Similarly, Lozovatsky et al. (2003) show an energy density of about 0.3–2 J/m^3 depending on the distance from the mid-ocean bottom topography ridge where tidal energy is converted to internal waves. We, therefore, consider the energy levels of our weakly and medium forcing cases to be in a range relevant to the dynamics of internal waves in the ocean. The simulated spectra in Fig. 1b show that the numerical eddy viscosity affects horizontal wavenumbers above 50 or so, where the spectra start decaying more rapidly beyond an inertial range not affected by dissipation.

2 Testing the assumptions behind the derivations of resonant wave theory

Different derivations of the RWIA rely on somewhat different assumptions, which are all based on the wave amplitudes changing on a timescale longer than the linear wave period. Derivations of the RWIA have been presented using a continuous or discrete vertical representation of the internal wave field, using Eulerian, Lagrangian, and isopycnal coordinates, as well as a Hamiltonian formulation, and more (Hasselmann, 1966; Kenyon, 1968; Müller and Olbers, 1975; McComas and Bretherton, 1977; McComas, 1977; Pomphrey et al., 1980; Phillips, 1981; Milder, 1982; Caillol and Zeitlin, 2000; L’vov and Tabak, 2001, 2004), see a helpful summary of approaches to deriving the kinetic equation of weak wave turbulence in Table 1 of L’vov et al. (2012). Regardless of the basic approach, all derivations then use a variant of the slowness assumption to derive the constraint on the frequencies of interacting waves. We present three different derivations of this constraint used in the literature and test the validity conditions for each, using our model simulations. We reproduce the full derivations of the kinetic equation from existing literature in the appendices and outline them here in order to present our results regarding the validity of each assumption.

Starting from the momentum, buoyancy, and continuity equations, one nondimensionalizes the equations (Appendix B) and derives (Appendix C) non-dimensional equations for the vorticity ($\zeta = u_z - w_x$) and buoyancy ($b = -g\rho/\rho_0$) in physical space, with (x, z) and (u, w) being the coordinates and velocities in the horizontal and vertical directions, respectively, and with ρ , ρ_0 , and g being the perturbation density relative to a specified linear mean stratification, a constant reference density, and gravity acceleration. Using the Fourier transform of the vorticity and the buoyancy, we define a wave amplitude $A_{s,\mathbf{k}}$ (e.g., Carnevale, 1981) and calculate it from the output of our DNS,

$$A_{s,\mathbf{k}} = \frac{1}{2}(\zeta_{\mathbf{k}}/k + sb_{\mathbf{k}}), \quad (1)$$

where k is the magnitude of the wavevector and $s = \pm 1$, corresponding to right and left propagating waves. The dynamics of the wave amplitude are described by,

$$\frac{\partial A_{a,\mathbf{k}}}{\partial t} + \mathcal{L}_{ab}A_{b,\mathbf{k}} = \frac{\epsilon}{(4\pi)^2} \int_{-\infty}^{\infty} d^2\mathbf{q} d^2\mathbf{p} \mathcal{M}_{abc}(\mathbf{k}, \mathbf{p}, \mathbf{q}) \delta(\mathbf{k} - \mathbf{p} - \mathbf{q}) A_{b,\mathbf{p}} A_{c,\mathbf{q}} + F_a(\mathbf{k}), \quad (2)$$

where t denotes the time, and a sum over repeated indices (b, c) is implied; note that when b is used as a subscript it is an index taking the values ± 1 rather than referring to the buoyancy. Here, \mathcal{L}_{ab} is a linear operator, $\mathcal{M}_{abc}(\mathbf{k}, \mathbf{p}, \mathbf{q})$ is a nonlinear interaction coefficient (Appendix C), and ϵ is a dimensionless parameter characterizing the ratio of the nonlinear and linear parts of the amplitude dynamics (Appendix B). The energy equation, in terms of the wave amplitudes in spectral space, is then (Appendix C),

$$\begin{aligned} \frac{\partial}{\partial t} (A_{a,\mathbf{k}} A_{a,\mathbf{k}}^*) &= \epsilon 2 \text{Re} \left(\frac{1}{4(2\pi)^2} \int_{-\infty}^{\infty} d^2\mathbf{q} d^2\mathbf{p} \right. \\ &\quad \left. \times \delta(\mathbf{k} - \mathbf{p} - \mathbf{q}) \mathcal{M}_{abc}(\mathbf{k}, \mathbf{p}, \mathbf{q}) A_{b,\mathbf{p}} A_{c,\mathbf{q}} A_{a,\mathbf{k}}^* \right) - 2 \text{Re} (L_{ab} A_{b,\mathbf{k}} A_{a,\mathbf{k}}^*) + 2 \text{Re} (F_a^*(\mathbf{k}) A_{a,\mathbf{k}}). \end{aligned} \quad (3)$$

The resonance condition requires that the nonlinear interaction term on the RHS of the energy equation, $\mathcal{M}_{abc}(\mathbf{k}, \mathbf{p}, \mathbf{k} - \mathbf{p}) A_{b,\mathbf{p}} A_{c,\mathbf{k}-\mathbf{p}} A_{a,\mathbf{k}}^*$, be strong only if

$$\Delta\omega(\mathbf{k}, \mathbf{p}, \mathbf{q}, a, b, c) = a\omega_{\mathbf{k}} - b\omega_{\mathbf{p}} - c\omega_{\mathbf{q}} = 0, \quad (4)$$

where $a, b, c = \pm 1$ indicate the wave phase propagation direction and frequencies are taken to be positive, in addition to the condition on the wavevectors imposed by the delta function $\delta(\mathbf{k} - \mathbf{p} - \mathbf{q})$. Fig. 2 shows the

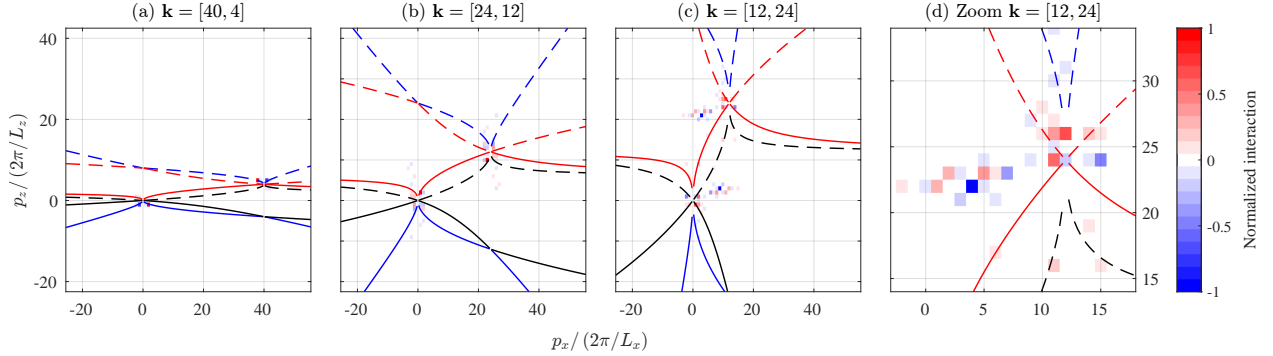


Figure 2: (a–c) Time-average of the interaction term ($M_{abc}(\mathbf{k}, \mathbf{p}, \mathbf{k} - \mathbf{p}) A_{b,\mathbf{p}} A_{c,\mathbf{k}-\mathbf{p}} A_{a,\mathbf{k}}^*$ in eq. (3)) for $\mathbf{k} = (40, 4)$, $(24, 12)$, and $(12, 24)$, for the weakly forced run, normalized (for each \mathbf{k}) by its maximum value. The color range corresponds only to a half of the range of values plotted to highlight weaker interactions. (d) A zoom into the region of $\mathbf{p} \sim \mathbf{k}$ for panel (c). The dashed and solid, blue, red, and black lines represent the different resonance curves.

time average of the nonlinear interaction term $M_{abc}(\mathbf{k}, \mathbf{p}, \mathbf{k} - \mathbf{p}) A_{b,\mathbf{p}} A_{c,\mathbf{k}-\mathbf{p}} A_{a,\mathbf{k}}^*$ in eq. (3) for the weakly forced simulation, for three different wavevectors \mathbf{k} . The resonant wavevectors satisfying $\Delta\omega(\mathbf{k}, \mathbf{p}, \mathbf{k} - \mathbf{p}, a, b, c) = 0$ are shown by the lines. The interaction term is shown by the color shading and is significant only for a small fraction of these resonant wavevectors. Interestingly, the strong interactions (darker blue or red pixels) occur for triads in which two wavevectors are large and one small (i.e., for $\mathbf{p} \approx \mathbf{k}$, or, equivalently, $\mathbf{q} \approx \mathbf{k}$). The parametric subharmonic instability and induced diffusion interactions (McComas and Bretherton, 1977) also involve a small wavevector mode. However, these special triad interactions are relevant only when the RWIA is valid, while we show below that the required conditions for the RWIA to hold are not met in our simulations. Another possible explanation of the dominant interactions in our weakly forced simulation (Fig. 2), between *forced* small wavevectors and larger ones, may be the generalized quasi-linear approximation (GQL, Marston et al., 2016). However, our stronger forced runs (Figs. G.2, G.4) show strong interactions even between unforced wavevectors, so it is not clear that GQL describes the dominant interactions for our three simulations.

In addition, some non-resonant interactions are stronger than most resonant interactions. These are better demonstrated in the zoomed-in Fig. 2d, in Fig. G.1 which shows a zoomed-in color range, and in Figs. G.2, G.3, G.4, and G.5 which show the interaction term for the two simulations with stronger forcing with a narrow color range. There, one can see darkly colored pixels away from the resonance curves and involving unforced wavevectors \mathbf{k}, \mathbf{p} , and \mathbf{q} . The values of the nondimensional nonlinearity parameter ϵ , (Appendix B) for the three simulations are small: 5×10^{-5} , 0.0001, and 0.0003, for the weak, intermediate, and strong forcing, respectively, suggesting that the RWIA should apply to all three runs, while our above interaction term plots suggest that this is not the case.

We now consider three different derivations of the RWIA starting from the above equations. The **first** is based on a formal two-timescale perturbation approach (see Benney and Saffman (1966), or as outlined in the context of the weak wave turbulence approach to internal waves in, e.g., Caillol and Zeitlin (2000), with the general multiple timescale perturbative method described in section 11.2 of Bender and Orszag (1978)) applied to the momentum equation (2). For this derivation, which is independent of the weak wave turbulence formalism, one assumes that the wave amplitude is a product of a slow amplitude varying as a function of $\tau = \epsilon t$ and a faster changing linear wave oscillatory part varying as a function of t ,

$$A_{a,\mathbf{k}} = \hat{A}_{a,\mathbf{k}}(\tau) e^{i a \omega_{\mathbf{k}} t}. \quad (5)$$

This decomposition requires that the slow amplitude $\hat{A}_{a,\mathbf{k}}(\tau)$ indeed varies slower than the oscillating exponent on the RHS. Under this assumption, the detailed derivation in Appendix D shows that a consistency

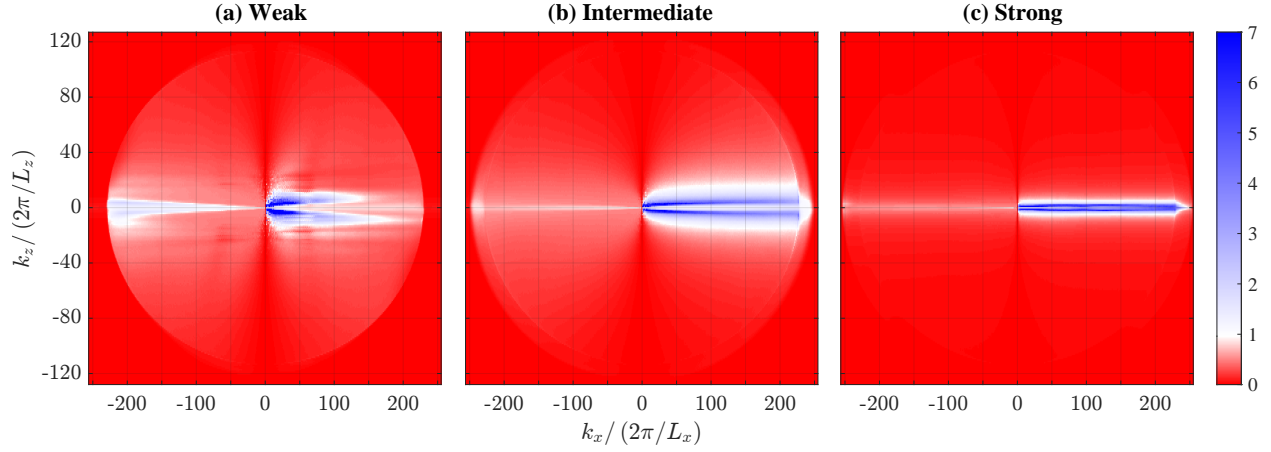


Figure 3: Testing the slow amplitude assumption used in the first derivation of the RWIA, requiring $V_1 \gg 1$, eq. (6). (a) weak, (b) intermediate, and (c) strong forcing.

condition must be satisfied for the perturbation approach to be valid for nondimensional times $t > 1/\epsilon$. The condition is represented by eq. (4), leading to the main result of the RWIA whose testing is our focus here. To test whether a slow amplitude approximation is consistent with our numerical simulations, we define a measure of the timescale of slow amplitude variations, $T(\hat{A}_{a,\mathbf{k}})$, relative to the wave period as $V_1(\mathbf{k}, a)$, and the self-consistency of the first derivation of the RWIA requires that this measure satisfies,

$$V_1(\mathbf{k}, a) = T(\hat{A}_{a,\mathbf{k}}) \frac{|\omega_{\mathbf{k}}|}{2\pi} = \left(\frac{2\pi}{[\hat{A}_{a,\mathbf{k}}]} \left[\frac{d\hat{A}_{a,\mathbf{k}}}{dt} \right] \right)^{-1} \frac{|\omega_{\mathbf{k}}|}{2\pi} \gg 1. \quad (6)$$

Here $[\cdot]$ indicates the RMS of the real part of the quantity in brackets (results for the imaginary part are similar). Fig. 3 shows V_1 for all the resolved wavevectors, and clearly, for nearly all wavevectors except perhaps those with a small vertical wavenumber, it is not larger than one, certainly not much larger. The reason for this is made clear in Fig. 4. Even for the relatively short period waves in panel (c), the slow amplitude envelope shown by the blue line is not smooth and its time scale is therefore not large. For the even longer-period waves in the other two panels, it is difficult to distinguish between the wave amplitude and what was supposed to be the slow amplitude.

There seems to be a self-consistency issue with the condition arising in this first derivation when the derivation is applied to a random wave field, that only resonant interactions are significant. The condition takes the form (Appendix D),

$$\delta(\mathbf{k} - \mathbf{p} - \mathbf{q}) M_{sab}(\mathbf{k}, \mathbf{p}, \mathbf{q}) \hat{A}_{a,\mathbf{p}}(\tau) \hat{A}_{b,\mathbf{q}}(\tau) \propto \delta(s\omega(\mathbf{k}) - a\omega(\mathbf{p}) - b\omega(\mathbf{q})). \quad (7)$$

For this condition to be satisfied for a given \mathbf{k} and letting $\mathbf{q} = \mathbf{k} - \mathbf{p}$, the amplitude of $\hat{A}_{b,\mathbf{p}}(\tau)$ must be small for \mathbf{p} away from the resonance, and large for the values of \mathbf{p} for which the resonance condition is satisfied. However, a specific \mathbf{p} might satisfy the resonance condition for one value $\mathbf{k} = \mathbf{k}_1$ and may be out of resonance for another $\mathbf{k} = \mathbf{k}_2$. Thus, the amplitude at any \mathbf{p} is required to be both large and small for the derivation to be valid. It is, therefore, not clear that this condition can be satisfied for a field of waves, regardless of the results of our numerical simulation.

The standard derivation of the RWIA, in the context of weak wave turbulence, is based on the energy rather than the amplitude equation and typically uses a Gaussian decomposition of a fourth-order amplitude product. The **second** derivation of the RWIA we consider is based on the energy equation, yet, avoids the Gaussian assumption, which we later consider in the third derivation. We proceed in this second derivation

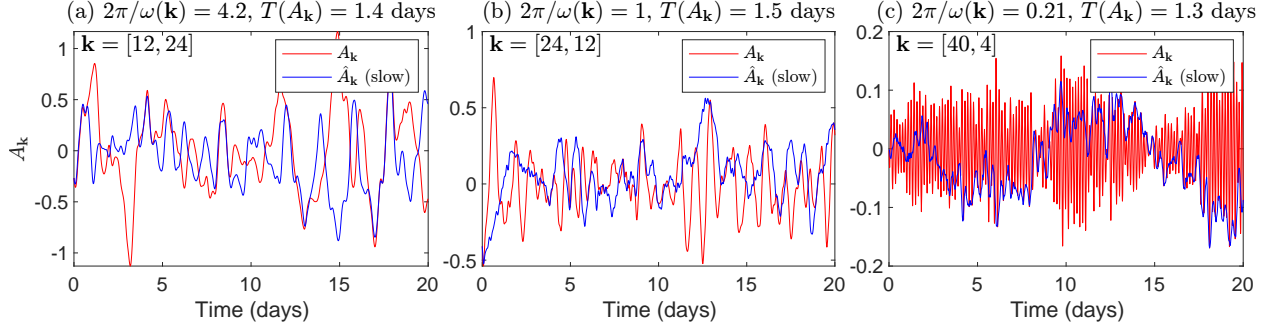


Figure 4: Time series of the fast and slow amplitudes of three particular wavenumbers.

by separating the wave amplitudes into $A_{a,\mathbf{k}}(t) = \hat{A}_{a,\mathbf{k}}(t)e^{ia\omega_{\mathbf{k}}t}$, temporally averaging the energy equation (3) over a time T , and neglecting dissipation and forcing terms (Appendix E),

$$\begin{aligned} \frac{1}{T} \left(\hat{A}_{a,\mathbf{k}} \hat{A}_{a,\mathbf{k}}^* \right) \Big|_0^T &= Re \left(\frac{2\epsilon}{(4\pi)^2} \int_{-\infty}^{\infty} d^2\mathbf{q} d^2\mathbf{p} \right. \\ &\times \delta(\mathbf{k} - \mathbf{p} - \mathbf{q}) \sum_{b,c} M_{abc}(\mathbf{k}, \mathbf{p}, \mathbf{q}) \times \frac{1}{T} \int_0^T \hat{A}_{b,\mathbf{p}} \hat{A}_{c,\mathbf{q}} \hat{A}_{a,\mathbf{k}}^* e^{i(-a\omega_{\mathbf{k}} + b\omega_{\mathbf{p}} + c\omega_{\mathbf{q}})t} dt \Big). \end{aligned} \quad (8)$$

Now assume that the product of the three slow amplitudes varies slower than the oscillating exponent in the last line of this equation. Under this assumption, we can write the averaged product (of the three amplitudes times the exponential term) there as a product of averages. In the limit $T \rightarrow \infty$, the average over the exponential term leads to the Kronecker delta, $\delta_{0,\Delta\omega}$, and thus to the resonance condition (denoting time average over a time T as $\overline{(\cdot)}$),

$$X \equiv Re \left(\overline{\hat{A}_{b,\mathbf{p}} \hat{A}_{c,\mathbf{q}} \hat{A}_{a,\mathbf{k}}^*} \times \frac{1}{T} \int_0^T e^{i\Delta\omega t} dt \right) \xrightarrow{T \rightarrow \infty} Re \left(\overline{\hat{A}_{b,\mathbf{p}} \hat{A}_{c,\mathbf{q}} \hat{A}_{a,\mathbf{k}}^*} \right) \delta_{0,\Delta\omega}. \quad (9)$$

In order to test the validity of this approximation, we examine the integral in the last line of eq. (8) before any approximations, $Y = Re \left(\frac{1}{T} \int_0^T \hat{A}_{b,\mathbf{p}} \hat{A}_{c,\mathbf{q}} \hat{A}_{a,\mathbf{k}}^* e^{i(-a\omega_{\mathbf{k}} + b\omega_{\mathbf{p}} + c\omega_{\mathbf{q}})t} dt \right)$ vs. X in eq. (9). The two quantities X and Y should be approximately the same for the RWIA derivation to be valid. In order to quantify the difference between the two, we use the following measure,

$$V_{2,a,b,c}(\mathbf{k}, \mathbf{p}, \mathbf{q}) = \frac{X_{a,b,c}(\mathbf{k}, \mathbf{p}, \mathbf{q}) - Y_{a,b,c}(\mathbf{k}, \mathbf{p}, \mathbf{q})}{\text{norm}(\mathbf{k}, a, b, c)}. \quad (10)$$

The normalization factor in the denominator is calculated as the maximum of $|X|$ and $|Y|$ over all \mathbf{p} values (for the specified a, b, c and \mathbf{k} , and where $\mathbf{q} = \mathbf{k} - \mathbf{p}$), and is defined as

$$\text{norm}(\mathbf{k}, a, b, c) = \max_{\mathbf{p}} (|X_{a,b,c}(\mathbf{k}, \mathbf{p}, \mathbf{q})|, |Y_{a,b,c}(\mathbf{k}, \mathbf{p}, \mathbf{q})|).$$

The normalization limits $V_{2,a,b,c}(\mathbf{k}, \mathbf{p}, \mathbf{q})$ to the range $[-2, 2]$. If the assumption justifying the replacement of the average of the product by the product of averages is valid, the measure V_2 should be much smaller than one. Fig. 5 shows V_2 for the weakly forced simulation (for the other two simulations, see Supplementary Figs. G.6 and G.7). In areas of the wavevector space where the interaction term is non-negligible (that is, for $\mathbf{p} \approx 0$ and for $\mathbf{q} = \mathbf{p} - \mathbf{k} \approx 0$, Fig. 2), the values of V_2 are large and close to their maximal absolute

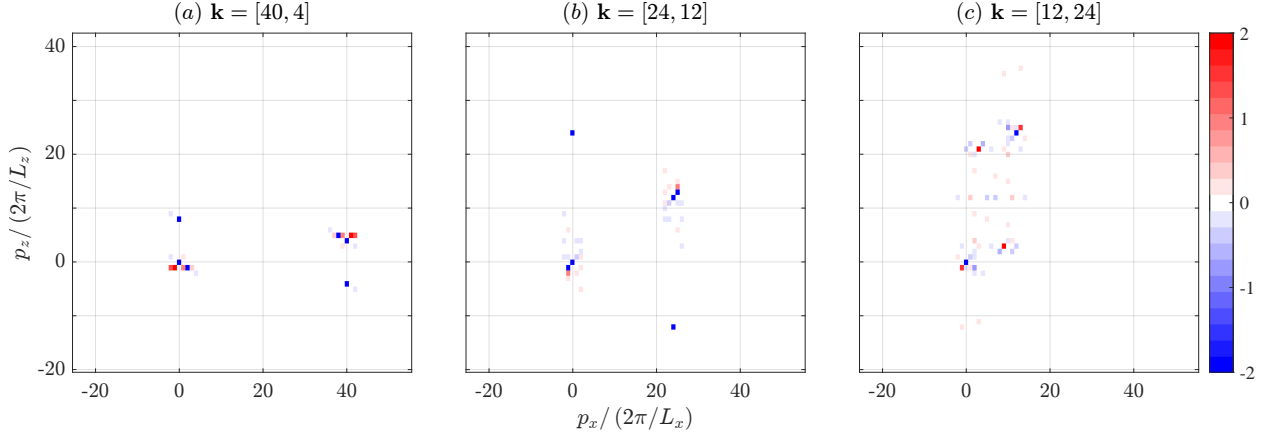


Figure 5: Testing whether the three-product of wave amplitudes varies slowly (criterion V_2 , eq. (10)) for the weak forcing case, for the wavevectors denoted in the titles of each panel.

value of 2, and are thus not consistent with this second derivation. While derivations in the literature simply assume $T \rightarrow \infty$, it is far from obvious what integration time T should be used in this test of the second derivation. Because our DNS are in a statistical steady state and we do not expect a significant trend in wave amplitudes, we choose a long integration time of 200 days. One might need to use a time that is a function of the wave periods appearing in the definition of X and Y . Yet our results indicate that the assumption of a slow amplitude is not easy to test and does not seem to hold in the context of this second derivation as well.

In the **third** and most commonly used approach to the derivation of the RWIA (used, for example, in the context of the application of the weak wave turbulence's kinetic equation to internal waves by L'vov et al. (2012) based on a canonical Hamiltonian approach, or in Nazarenko (2011) where the derivation is applied to the generating function), one derives an equation for the time derivative of the triple product appearing in the energy equation (3), where the RHS of this equation contains a four-product of the wave amplitudes (Appendix F). One then applies an ensemble average, uses a Gaussian decomposition of the four-product, assumes a spatial translation invariance, and assumes that right and left-propagating waves are uncorrelated. The RHS of the energy equation then contains a time integral over products of the energy multiplied by $e^{i\Delta\omega t}$ (eq. F-36). This integral is simplified (e.g., Caillol and Zeitlin, 2000; L'vov et al., 2012), assuming that the ensemble-averaged energy spectrum varies over a timescale that is longer than the wave periods. This leads to an integral over $e^{i\Delta\omega t}$ and thus to a delta-function factor $\delta(\Delta\omega)$, representing the resonance condition, leading to the final resonant kinetic equation. However, a more proper assumption for the validity of this derivation may be that the timescale of the energy spectrum variations should be much larger than the timescale of the oscillating term represented by $2\pi/\Delta\omega$. Letting T be the timescale over which the energy varies (defined more precisely below), the condition for this third derivation to be valid is

$$V_3(\mathbf{k}, \mathbf{p}, a, b, c) = \frac{2\pi}{\Delta\omega(\mathbf{k}, \mathbf{p}, \mathbf{k} - \mathbf{p}, a, b, c)} / T \ll 1. \quad (11)$$

Given that, by definition, $\Delta\omega = 0$ on resonance curves, eq. (11) cannot be satisfied for resonant interactions. Supplementary Fig. G.8 shows V_3 , using a somewhat arbitrary $T = 1$ day timescale (to be improved on shortly), demonstrating that V_3 is also not small *near* the resonance curves, as expected. If significant interactions occur *near* resonance curves, rather than only *on* the curves, as has been suggested (L'vov et al., 1997, 2012), this condition needs to be satisfied at least near the curves, even if it cannot be satisfied on the curves, for this derivation to be self-consistent. To test the validity of the assumption underlying the third derivation near the resonance curves, we first calculate the time scale of energy changes at wavevector \mathbf{k} due to nonlinear interactions with wavenumbers \mathbf{p} and \mathbf{q} . The time scale is based on each term in the energy

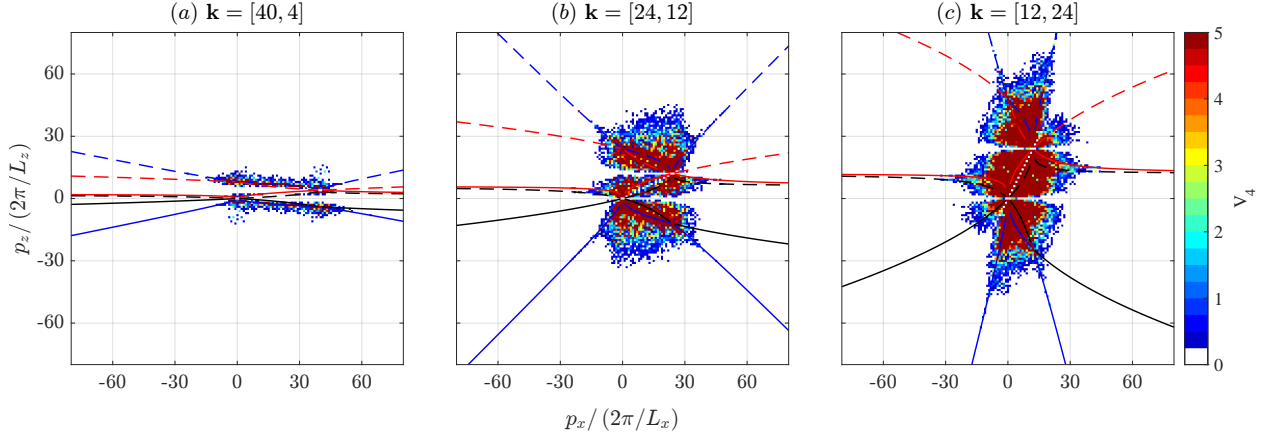


Figure 6: The ratio between the nonlinear timescale and the wave triad timescale (V_4). V_4 should be much smaller than 1 for the RWIA to be valid (eq. 13). The ratio is presented for three wavevectors, $\mathbf{k} = (40, 4)$, $(24, 12)$, and $(12, 24)$.

equation in wavenumber space (3), as the averaged energy divided by the average of the energy transfer term,

$$T_{a,b,c}(\mathbf{k}, \mathbf{p}, \mathbf{q}) = \delta_{\mathbf{k}, \mathbf{p}+\mathbf{q}} \overline{A_{a,\mathbf{k}} A_{a,\mathbf{k}}^*} \times \left| \frac{1}{2(2\pi)^2} M_{abc}(\mathbf{k}, \mathbf{p}, \mathbf{q}) \text{Re} \left(\overline{A_{b,\mathbf{p}} A_{c,\mathbf{q}} A_{a,\mathbf{k}}^*} \right) \right|^{-1} \quad (12)$$

We use time averages denoted by $\overline{(\cdot)}$ rather than ensemble averages to define and calculate this timescale using our numerical simulations. There are four such timescales for each value of a , corresponding to $b = \pm 1$, $c = \pm 1$, and thus to the four terms appearing on the RHS of the energy equation. For the third derivation to be consistent, all four timescales must be larger than the linear wave period, as pointed out by (L’vov et al., 2012). It is common to use a less restrictive measure of the time scale based on the rate due to all terms combined (Holloway, 1980; L’vov et al., 2012; Eden et al., 2020), yet the validity of the approximation depends on the time scale due to each of the four terms being long. In an inertial range where energy arrives from small wavenumbers and flows to large wavenumbers, the total time-averaged transfer vanishes in a statistical steady state, and the resulting time scale is infinite yet not relevant to the validity of the approximation. We thus define a measure of the slowness of the nonlinear dynamics based on these four time-scales,

$$V_4(\mathbf{k}, \mathbf{p}, \mathbf{q}, a) = \max_{b,c} \frac{2\pi/\Delta\omega(\mathbf{k}, \mathbf{p}, \mathbf{q}, a, b, c)}{T_{a,b,c}(\mathbf{k}, \mathbf{p}, \mathbf{q})} \ll 1. \quad (13)$$

The consistency criterion for the third derivation of the RWIA is therefore based on the maximum over the four terms ($b, c = \pm 1$) rather than on their sum. This quantity is shown in Fig. 6 for three wavevectors (\mathbf{k}) for the weakly forced simulation. It is shown as a function of $\mathbf{p} = (p_x, p_z)$, taking $\mathbf{q} = \mathbf{k} - \mathbf{p}$. Small values of V_4 are shown in white, and it is clearly not much smaller than 1 in the relevant regions of wavenumber space where the interactions occur (Fig. 2). This, together with the fact that the condition cannot be satisfied for strictly resonant wavevectors, leads us to conclude that the third derivation of the resonant wave interaction approximation is not consistent with the results of our simulations. The results for the stronger forcing cases are similar (Figs. G.9 and G.10).

3 Discussion and conclusions

Previous studies applied the RWIA and the weak wave turbulence kinetic equation to internal waves (e.g., McComas and Bretherton, 1977; Caillol and Zeitlin, 2000; Kenyon, 1968). The weak interaction hypothesis behind the kinetic equation was found to be inconsistent with observations (Holloway, 1980), while the self-consistency of the kinetic equation was carefully examined by (L’vov et al., 2012). Yet, to the best of our knowledge, no prior effort has examined whether the nonlinear dynamics due to the interaction of internal waves are consistent with the assumptions underlying the derivation of the RWIA, and whether these dynamics satisfy the resonance constraint on the frequencies of triads interacting internal waves.

We find that none of the three derivations considered is consistent with our direct numerical simulations because the assumption that the wave amplitudes or energy slowly vary is violated even for our weakest forced simulation, and the timescale of energy and amplitude changes at a given wavevector is therefore not much larger than the wave period, as required by the derivation. The rapidly varying amplitudes, despite the very weak nonlinear interaction, suggest that it may not be completely justified to think of the fluid motion as interacting linear internal waves, as such a description implies slowly varying amplitudes. Furthermore, for two of the derivations (the first and third considered above), we found that there seem to be self-inconsistencies. We conclude that the RWIA does not seem to be consistent with the interactions as deduced from our direct numerical simulations.

Many of our results, while carefully derived, rely on the adequacy and relevance of the direct numerical simulations employed here. The idealizations employed here, including the double periodic 2d domain, are similar to those used in recent simulations of internal ocean waves (Sugiyama et al., 2009; Eden et al., 2019a; Chen et al., 2019). Yet, the simulations span a range of no more than 1–2 orders of magnitude of wavenumbers that are not dominated by the numerical model viscosity. We do not include the Coriolis force nor the abundant near-inertial motions generated in the ocean by the winds at the surface by the interaction of internal tides with topography. Our use of 2d vs. 3d simulations means that the number of resonant interactions in any range of wave-frequencies is lower, potentially weakening the resonant interactions (Lvov et al., 2006), and we further discuss this in the following paragraph. The use of 2d simulations also implies that we do not resolve vertical vorticity due to the horizontal shear of the horizontal velocity, which was found to play an important role in scattering internal wave energy (Cox et al., 2022; Savva et al., 2021; Kafiabad et al., 2019; Young, 2021). Our simulations are meant to examine the RWIA in the simplest configuration, and their applicability to the real ocean is not obvious.

Furthermore, the RWIA involves taking two limits: the system size going to infinity and the nonlinearity being very weak (e.g., Nazarenko, 2011). In a numerical simulation, the resolved wavenumbers are discrete and cannot be expected to lie exactly on the resonant curves. This might suggest that a discrete simulation cannot be used to test the RWIA. However, it was shown that nonlinear interactions lead to the broadening of the resonance curves to include near-resonant interactions (L’vov et al., 1997, 2012) within the RWIA. This broadening implies that under the assumptions of the RWIA, near-resonance interactions are expected to dominate the energy transfer and allow an energy cascade to develop (Lvov et al., 2006). It is difficult to estimate a priori the specific broadening for a given strength of the nonlinear interactions and numerical resolution. It is also not known theoretically what number of near-resonant interactions is required for weak wave turbulence to be well-represented on a finite grid. In order to address these issues, we invoke the estimates of the nonlinear broadening of resonance curves estimated by L’vov et al. (2012). They find that a Lorentzian broadening, with the width set to 0.5 times the sum of frequencies of the three interacting waves, leads to a self-consistent Boltzmann ratio. We analyzed their suggested Lorentzian weight applied to near-resonance wavenumbers and considered any triad whose weight is larger than 0.75 to be an activated near-resonance interaction. For the three wavenumbers considered in our different figures, this broadening leads to 35%–75% of the wavenumbers being activated(!). It seems, therefore, that our simulations contain a sufficient number of activated interactions within the near-resonance range of the RWIA for a realistic level of nonlinearity in observed ocean internal waves. Another mechanism that leads to the broadening of resonances and to the activation of near-resonant interactions was discussed by Annenkov and Shrira (2006) and Janssen (2003). They point out that the limit of infinite integration time that leads to the delta function

corresponding to the resonant frequencies (see definition and limit of the function $\delta_T(\Delta\omega)$ in eqs. E-30 and E-31) is not physical as the wave amplitudes vary over such a long time due to nonlinear interactions. As a result, they consider a finite time limit in which this function maintains a finite width and leads to the inclusion of near-resonance interactions to be more realistic. They conclude that this broadening justifies the application of the kinetic equation to the analysis of a finite-resolution DNS. A related broadened-resonance analysis and a resulting generalized kinetic equation were applied to the parametric subharmonic instability by Onuki and Hibiya (2019). Any numerical simulations cannot strictly satisfy the large-box limit required for the kinetic equation to hold in the sense that this limit allows for enough strict resonances to exist (Nazarenko, 2011). Yet, the above discussion of processes leading to the broadening of resonances means that even at a finite system size, we expect to have enough activated resonances. While this discussion suggests that the discreteness and the finite domain size of the numerical simulation may not be major issues for our results, it would be good to use the same analysis approach with numerical simulations that use a much higher resolution and a larger domain size.

It is important to note that while we find issues with the assumptions used to derive the kinetic equation when tested in an idealized framework, it has been used successfully for explaining observed internal ocean characteristics, such as internal tide damping rates (e.g., Onuki and Hibiya, 2018; Olbers et al., 2020); these studies showed that the kinetic equation, formulated in terms of vertical wave modes, can correctly estimate the decay rates of internal waves via the parametric subharmonic instability and the transfer of tidal energy to the wave continuum. Similarly, L’vov and Tabak (2001) showed that the energy kinetic equation, based on Hamiltonian formalism, results in a GM-like energy spectrum. Pan et al. (2020) showed that in a high-resolution realistic simulation, scale-separated interactions such as induced diffusion are the most important mechanisms for the formation of the power-law spectrum. This last result is consistent with our finding of strong interactions with low wave numbers in Fig. 2, although we note that non-resonant interactions with low wave numbers are also important in our simulations. We have also not addressed a recent alternative derivation of the kinetic equation based on large deviations theory (Guioth et al., 2022).

We note that none of the idealizations used here and model limitations would necessarily mean that the RWIA should not have applied to the simulation results, given that the measure of the nonlinearity (ϵ above) is very small for all our simulations and this weak nonlinearity is the basis for the slowness assumption used in all derivations of the RWIA. Our findings, while perhaps only suggestive due to the limited numerical resolution, call for further testing of the assumptions underlying the RWIA in more sophisticated simulations following the methodology outlined here.

acknowledgments. We thank Kraig Winters for making the code of `flow_solve` available. GB thanks Ester Levi for a lifelong inspiration. ET thanks the Weizmann Institute for its hospitality during parts of this work, and has been funded by the NSF Climate Dynamics Program (joint NSF/NERC) grant AGS-1924538.

References

- Sergei Yu Annenkov and Victor I Shrira. Role of non-resonant interactions in the evolution of nonlinear random water wave fields. *Journal of Fluid Mechanics*, 561:181–207, 2006.
- C. M. Bender and S. A. Orszag. *advanced mathematical methods for scientists and engineers*. McGraw-Hill, 1978.
- D. J. Benney and P. G. Saffman. Nonlinear interactions of random waves in a dispersive medium. *Philosophical Transactions of the Royal Society A*, 289(1418):301–320, 1966.
- F. Bryan. Parameter sensitivity of primitive equation ocean general circulation models. *Journal of Physical Oceanography*, 17:970–985, 1987.
- Ph. Caillol and V. Zeitlin. Kinetic equations and stationary energy spectra of weakly nonlinear internal gravity waves. *Dynamics of atmospheres and oceans*, 32(2):81–112, 2000.
- J. L. Cairns and G. O. Williams. Internal wave observations from a midwater float, 2. *Journal of Geophysical Research*, 81:1943–1950, 1976.
- G. F. Carnevale. Statistical field theory and the internal wave problem. In *AIP Conference Proceedings*, volume 76, pages 307–320. American Institute of Physics, 1981.
- Z. Chen, S. Chen, Z. Liu, J. Xu, J. Xie, Y. He, and S. Cai. Can tidal forcing alone generate a GM-like internal wave spectrum? *Geophysical Research Letters*, 46(24):14644–14652, 2019. doi: <https://doi.org/10.1029/2019GL086338>.
- Michael R. Cox, Hossein A. Kafiabad, and Jacques Vanneste. Inertia-gravity-wave diffusion by geostrophic turbulence: the impact of flow time dependence, 2022. URL <https://arxiv.org/abs/2207.09386>.
- R. E. Davis and A. Acrivos. The stability of oscillatory internal waves. *Journal of Fluid Mechanics*, 30(4):723–736, 1967.
- Wenjing Dong, Oliver Bühler, and K Shafer Smith. Frequency diffusion of waves by unsteady flows. *Journal of Fluid Mechanics*, 905, 2020.
- C. Eden, M. Chouksey, and D. Olbers. Mixed rossby-gravity wave-wave interactions. *Journal of Physical Oceanography*, 49(1):291 – 308, 2019a. doi: 10.1175/JPO-D-18-0074.1. URL <https://journals.ametsoc.org/view/journals/phoc/49/1/jpo-d-18-0074.1.xml>.
- C. Eden, F. Pollmann, and D. Olbers. Numerical evaluation of energy transfers in internal gravity wave spectra of the ocean. *Journal of Physical Oceanography*, 49(3):737 – 749, 2019b. doi: 10.1175/JPO-D-18-0075.1.
- C. Eden, F. Pollmann, and D. Olbers. Towards a global spectral energy budget for internal gravity waves in the ocean. *Journal of Physical Oceanography*, 50(4):935–944, 2020.
- C. Garrett and W. Munk. Space-time scales of internal waves: A progress report. *Journal of Geophysical Research*, 80:291–297, 1975.
- C. Garrett and W. Munk. Internal waves in the ocean. *Annual Review of Fluid Mechanics*, 11:339–369, 1979.
- C. Garrett and W. H. Munk. Space-time scales of internal waves. *Geophys. Fluid Dyn.*, 2:225–264, 1972.
- Jules Guioth, Freddy Bouchet, and Gregory L Eyink. Path large deviations for the kinetic theory of weak turbulence. *Journal of Statistical Physics*, 189(2):20, 2022.

- K. Hasselmann. On the non-linear energy transfer in a gravity-wave spectrum part 1. general theory. *Journal of Fluid Mechanics*, 12(4):481–500, 1962.
- K. Hasselmann. Feynman diagrams and interaction rules of wave-wave scattering processes. *Reviews of Geophysics*, 4(1):1–32, 1966. doi: <https://doi.org/10.1029/RG004i001p00001>. URL <https://agupubs.onlinelibrary.wiley.com/doi/abs/10.1029/RG004i001p00001>.
- E. Herbert, N. Mordant, and E. Falcon. Observation of the nonlinear dispersion relation and spatial statistics of wave turbulence on the surface of a fluid. *Phys. Rev. Lett.*, 105(14):144502, 2010.
- G. Holloway. Oceanic internal waves are not weak waves. *Journal of Physical Oceanography*, 10(6):906–914, 1980.
- Peter AEM Janssen. Nonlinear four-wave interactions and freak waves. *Journal of Physical Oceanography*, 33(4):863–884, 2003.
- Hossein A Kafiabad, Miles AC Savva, and Jacques Vanneste. Diffusion of inertia-gravity waves by geostrophic turbulence. *Journal of Fluid Mechanics*, 869, 2019.
- K. E. Kenyon. Wave-wave interactions of surface and internal waves. *Journal of Marine Research*, 26(3):208, 1968.
- Arnaud Le-Boyer and Matthew H Alford. Variability and sources of the internal wave continuum examined from global moored velocity records. *Journal of Physical Oceanography*, 51(9):2807–2823, 2021.
- M. D. Levine. A modification of the Garrett-Munk internal wave spectrum. *Journal of Physical Oceanography*, 32(11):3166–3181, 2002.
- I. D. Lozovatsky, E. G. Morozov, and H. J. S. Fernando. Spatial decay of energy density of tidal internal waves. *Journal of Geophysical Research: Oceans*, 108(C6), 2003.
- V. S. L’vov, Y. L’vov, A. C. Newell, and V. Zakharov. Statistical description of acoustic turbulence. *Phys. Rev. E*, 56:390–405, Jul 1997. doi: 10.1103/PhysRevE.56.390. URL <https://link.aps.org/doi/10.1103/PhysRevE.56.390>.
- Y. L’vov and E. G. Tabak. A hamiltonian formulation for long internal waves. *Physica D: Nonlinear Phenomena*, 195(1-2):106–122, 2004.
- Y. V. L’vov and E. G. Tabak. Hamiltonian formalism and the Garrett-Munk spectrum of internal waves in the ocean. *Phys. Rev. Lett.*, 87(16):168501, 2001.
- Y. V. L’vov, K. L. Polzin, and E. G. Tabak. Energy spectra of the ocean’s internal wave field: Theory and observations. *Phys. Rev. Lett.*, 92(12):128501, 2004.
- Y. V. L’vov, K. L. Polzin, and N. Yokoyama. Resonant and near-resonant internal wave interactions. *Journal of Physical Oceanography*, 42(5):669–691, 2012.
- Yuri V Lvov, Sergey Nazarenko, and Boris Pokorni. Discreteness and its effect on water-wave turbulence. *Physica D: Nonlinear Phenomena*, 218(1):24–35, 2006.
- J. B. Marston, G. P. Chini, and S. M. Tobias. Generalized quasilinear approximation: Application to zonal jets. *Phys. Rev. Lett.*, 116:214501, May 2016. doi: 10.1103/PhysRevLett.116.214501. URL <https://link.aps.org/doi/10.1103/PhysRevLett.116.214501>.
- C. H. McComas. Equilibrium mechanisms within the oceanic internal wave field. *Journal of Physical Oceanography*, 7(6):836–845, 1977.

- C. H. McComas and F. P. Bretherton. Resonant interaction of oceanic internal waves. *Journal of Geophysical Research*, 82:1397–1412, 1977.
- D. M. Milder. Hamiltonian dynamics of internal waves. *Journal of Fluid Mechanics*, 119:269–282, 1982.
- P. Müller and D. J. Olbers. On the dynamics of internal waves in the deep ocean. *Journal of Geophysical Research*, 80:3848–3860, 1975.
- Peter Müller, Greg Holloway, Frank Henyey, and Neil Pomphrey. Nonlinear interactions among internal gravity waves. *Reviews of Geophysics*, 24(3):493–536, 1986.
- W. Munk and C. Wunsch. Abyssal recipes II: energetics of tidal and wind mixing. *Deep-sea Research Part I-oceanographic Research Papers*, 45(12):1977–2010, December 1998.
- S. Nazarenko. *Wave turbulence*, volume 825. Springer Science & Business Media, 2011.
- M. Nikurashin and R. Ferrari. Overturning circulation driven by breaking internal waves in the deep ocean. *Geophysical Research Letters*, 40(12):3133–3137, 2013.
- Dirk Olbers, Friederike Pollmann, and Carsten Eden. On psi interactions in internal gravity wave fields and the decay of baroclinic tides. *Journal of Physical Oceanography*, 50(3):751–771, 2020.
- Yohei Onuki and Toshiyuki Hibiya. Decay rates of internal tides estimated by an improved wave-wave interaction analysis. *Journal of Physical Oceanography*, 48(11):2689–2701, 2018.
- Yohei Onuki and Toshiyuki Hibiya. Parametric subharmonic instability in a narrow-band wave spectrum. *Journal of Fluid Mechanics*, 865:247–280, 2019.
- Y. Pan, B. K. Arbic, A. D. Nelson, D. Menemenlis, W. R. Peltier, W. Xu, and Y. Li. Numerical investigation of mechanisms underlying oceanic internal gravity wave power-law spectra. *Journal of Physical Oceanography*, 50(9):2713–2733, 2020.
- O. M. Phillips. Wave interactions-the evolution of an idea. *Journal of Fluid Mechanics*, 106:215–227, 1981.
- Friederike Pollmann. Global characterization of the ocean’s internal wave spectrum. *Journal of Physical Oceanography*, 50(7):1871–1891, 2020.
- K. L. Polzin and Y. V. Lvov. Toward regional characterizations of the oceanic internal wavefield. *Reviews of Geophysics*, 49(4), 2011. doi: <https://doi.org/10.1029/2010RG000329>.
- N. Pomphrey, J. D. Meiss, and K. M. Watson. Description of nonlinear internal wave interactions using langevin methods. *Journal of Geophysical Research: Oceans*, 85(C2):1085–1094, 1980.
- Christopher L. Sabine, Richard A. Feely, Nicolas Gruber, Robert M. Key, Kitack Lee, John L. Bullister, Rik Wanninkhof, C. S. Wong, Douglas W. R. Wallace, Bronte Tilbrook, Frank J. Millero, Tsung-Hung Peng, Alexander Kozyr, Tsueno Ono, and Aida F. Rios. The oceanic sink for anthropogenic CO₂. *Science*, 305(5682):367–371, 2004. doi: 10.1126/science.1097403. URL <https://www.science.org/doi/abs/10.1126/science.1097403>.
- Miles AC Savva, Hossein A Kafiabad, and Jacques Vanneste. Inertia-gravity-wave scattering by three-dimensional geostrophic turbulence. *Journal of Fluid Mechanics*, 916, 2021.
- Y. Sugiyama, Y. Niwa, and T. Hibiya. Numerically reproduced internal wave spectra in the deep ocean. *Geophysical research letters*, 36(7), 2009.
- KB Winters, JA MacKinnon, and Bren Mills. A spectral model for process studies of rotating, density-stratified flows. *Journal of Atmospheric and Oceanic Technology*, 21(1):69–94, 2004.

- C. Wunsch and S. Webb. The climatology of deep ocean internal waves. *Journal of Physical Oceanography*, 9(2):235–243, 1979.
- William R Young. Inertia-gravity waves and geostrophic turbulence. *Journal of Fluid Mechanics*, 920, 2021.
- V. E. Zakharov. Weak turbulence in media with a decay spectrum. *Journal of Applied Mechanics and Technical Physics*, 6(4):22–24, 1965.
- V. E. Zakharov, V. S. L’vov, and G. Falkovich. *Kolmogorov spectra of turbulence I: Wave turbulence*. Springer Science & Business Media, 2012.

A Simulation details

Numerical simulations are performed with a 2d double-periodic configuration of the flow solve pseudospectral model (Winters et al., 2004). The domain size is $L_x = 100$ km in the horizontal direction and $L_z = 1$ km in the vertical direction, using 512 grid points in the horizontal direction and 256 in the vertical. A linear basic stratification is prescribed such that the Brunt–Väisälä buoyancy frequency is $N = 2\pi/30$ minutes⁻¹ (see section B), and the equations represent the full nonlinear dynamics of perturbations to this stratification. We seek maximal simplification and set the Coriolis force to zero. Each integration was carried out to a statistical steady state, and then for 200 more days, which were used for the analysis presented. Our analysis is based on a high-frequency sampling of the model output at an interval of 18 s, allowing us to resolve all relevant motions. The time step used for the integration is 1 s. In all simulations, we used $\rho_0 = 1000$ kg/m³.

We use three runs with different red noise (in time) stochastic forcing that is applied only to small wavenumbers of $0 < (L_x|k_x|, L_z|k_z|)/2\pi < 3$ where $\mathbf{k} = (k_x, k_z)$ is the wavevector. The forcing is applied to the buoyancy equation, eq. (B-2) (no forcing was applied directly to the momentum equations, eq. (B-1)), has the structure of waves that are solutions to the linearized equations. The amplitude of these driving waves, for each wavevector, was set using a temporally correlated red-color noise with a 12-min correlation time. We performed an additional simulation with a longer, 1-day, correlation time of the stochastic forcing to verify that it does not change the conclusions outlined in the paper. Specifically, the rapid fluctuations of the slow amplitude, shown in Fig. 4, appear also for the longer correlation time of the forcing. The stochastic forcing amplitudes of the different wavevectors were uncorrelated. The standard deviation of the medium forcing amplitude was six times larger than that of the weak one, and the forcing of the strong run was nine times that of the weakly forced run.

The eddy viscosity and diffusivity were set to the minimal values ensuring that a statistical steady state is achieved without numerical noise in the solution. The values used for the horizontal and vertical eddy viscosity are: $\tilde{\nu}_x = 0.1, 0.2, 0.2$ m²/s and $\tilde{\nu}_z = 3 \times 10^{-6}, 3 \times 10^{-5}, 3 \times 10^{-5}$ m²/s, for the weak, medium, and strongly forced simulations, respectively. The diffusivity was assumed to be isotropic and was set to $\tilde{\kappa}_x = \tilde{\kappa}_z = 3 \times 10^{-6}, 3 \times 10^{-5}, 3 \times 10^{-5}$ m²/s, for the weak, medium, and strongly forced simulations, respectively.

B Nondimensionalization

The dimensional momentum equations in terms of dimensional variables denoted with $(\tilde{\cdot})$ are

$$\begin{aligned}\tilde{u}_{\tilde{t}} + \tilde{\mathbf{u}} \cdot \tilde{\nabla} \tilde{u} &= -\frac{1}{\rho_0} \tilde{p}_{\tilde{x}} + \tilde{\nu}_x \frac{\partial^2}{\partial \tilde{x}^2} \tilde{u} + \tilde{\nu}_z \frac{\partial^2}{\partial \tilde{z}^2} \tilde{u} + \tilde{f}^{(x)}(\tilde{\mathbf{x}}, \tilde{t}), \\ \tilde{w}_{\tilde{t}} + \tilde{\mathbf{u}} \cdot \tilde{\nabla} \tilde{w} &= -\frac{1}{\rho_0} \tilde{p}_{\tilde{z}} - \tilde{b} + \tilde{\nu}_x \frac{\partial^2}{\partial \tilde{x}^2} \tilde{w} + \tilde{\nu}_z \frac{\partial^2}{\partial \tilde{z}^2} \tilde{w} + \tilde{f}^{(z)}(\tilde{\mathbf{x}}, \tilde{t}).\end{aligned}\tag{B-1}$$

Here, $\tilde{\mathbf{u}} = [\tilde{u}, \tilde{w}]$ is the velocity vector. The equation for the buoyancy $\tilde{b} = -g\rho/\rho_0$ is

$$\tilde{b}_{\tilde{t}} + \tilde{\mathbf{u}} \cdot \tilde{\nabla} \tilde{b} + \tilde{w} \tilde{b}_z = \tilde{\kappa}_x \frac{\partial^2}{\partial \tilde{x}^2} \tilde{b} + \tilde{\kappa}_z \frac{\partial^2}{\partial \tilde{z}^2} \tilde{b} + \tilde{f}^{(b)}(\tilde{\mathbf{x}}, \tilde{t}).\tag{B-2}$$

The incompressibility implies

$$\tilde{u}_x + \tilde{w}_z = 0.\tag{B-3}$$

In our direct numerical simulations, we impose a constant mean stratification which dictates the Brunt–Väisälä buoyancy frequency, \tilde{N} , as $\tilde{b}_z = \tilde{N}^2$.

In order to nondimensionalize the equations, we choose the following length, time, and velocity scales,

$$\tilde{x} = xL_x; \quad \tilde{z} = L_z z; \quad \tilde{t} = t/N; \quad \tilde{u} = u_0 u; \quad \tilde{w} = w_0 w = u_0 \frac{L_z}{L_x} w;,\tag{B-4}$$

and the nondimensionalization of the pressure and buoyancy are given by

$$\begin{aligned}\tilde{p} &= p_0 p; p_0 = \rho_0 L_x N u_0 = \rho_0 \frac{L_z}{T} w_0 \\ \tilde{b} &= b_0 b; b_0 = N w_0 = \frac{L_z}{L_x} u_0 N.\end{aligned}\tag{B-5}$$

Applying this to the momentum equations, one finds

$$\begin{aligned}u_t + \epsilon \mathbf{u} \cdot \nabla u &= -p_x + \left(\nu_x \frac{\partial^2 u}{\partial x^2} + \nu_z \frac{\partial^2 u}{\partial z^2} \right) + f^{(x)}(\mathbf{x}, t); \\ w_t + \epsilon \mathbf{u} \cdot \nabla w &= -p_z - b + \left(\nu_x \frac{\partial^2 w}{\partial x^2} + \nu_z \frac{\partial^2 w}{\partial z^2} \right) + f^{(z)}(\mathbf{x}, t); \\ b_t + \epsilon \mathbf{u} \cdot \nabla b - w &= \left(\kappa_x \frac{\partial^2 b}{\partial x^2} + \kappa_z \frac{\partial^2 b}{\partial z^2} \right) + f^{(b)}(\mathbf{x}, t); \\ u_x + w_z &= 0,\end{aligned}\tag{B-6}$$

where we defined the components of the dimensionless anisotropic eddy kinematic viscosity $\nu_x = \tilde{\nu}_x / N L_x^2$; $\nu_z = \tilde{\nu}_z / N L_z^2$; the components of the dimensionless anisotropic eddy diffusivity, $\kappa_x = \tilde{\kappa}_x / N L_x^2$; $\kappa_z = \tilde{\kappa}_z / N L_z^2$; and the dimensionless forces

$$f^{(x)}(\mathbf{x}, t) = \frac{1}{N u_0} \tilde{f}^{(x)}(\tilde{\mathbf{x}}, \tilde{t}); \quad f^{(z)}(\mathbf{x}, t) = \frac{1}{N w_0} \tilde{f}^{(z)}(\tilde{\mathbf{x}}, \tilde{t}); \quad f^{(b)}(\mathbf{x}, t) = \frac{1}{N b_0} \tilde{f}^{(b)}(\tilde{\mathbf{x}}, \tilde{t}).$$

The nondimensional parameter multiplying the nonlinear terms is

$$\epsilon = u_0 / N L_x.\tag{B-7}$$

The velocity scale appearing here is calculated as the RMS horizontal velocity for each run, while L_x and L_z are the horizontal and vertical basins' extents, respectively.

C Derivation of the energy equation in spectral space

Based on the nondimensional equations derived in the previous section (eqs. (B-6)) we introduce a stream function ψ such that $u = \psi_z$; $w = -\psi_x$, and letting the vorticity be $\zeta = u_z - w_x = \nabla^2 \psi$. Take the curl of the momentum equations to derive a vorticity equation and rewrite the buoyancy equation to find

$$\begin{aligned}\zeta_t - (\nu_x \zeta_{xx} + \nu_z \zeta_{zz}) + b_x &= \epsilon J(\psi, \zeta) + f^\zeta(\mathbf{x}, t) \\ b_t - (\kappa_x b_{xx} + \kappa_z b_{zz}) - \psi_x &= \epsilon J(\psi, b) + f^b(\mathbf{x}, t).\end{aligned}\tag{C-8}$$

Here, $J(a, b) \equiv a_x b_z - a_z b_x$. Fourier transforming eqs. (C-8) yields

$$\begin{aligned}\dot{\zeta}_{\mathbf{k}} + (\nu_x k_x^2 + \nu_z k_z^2) \zeta_{\mathbf{k}} + i k_x b_{\mathbf{k}} &= \epsilon (2\pi)^{-2} \int_{-\infty}^{\infty} d^2 \mathbf{p} d^2 \mathbf{q} \delta(\mathbf{p} + \mathbf{q} - \mathbf{k}) (p_x q_z - p_z q_x) p^{-2} \zeta_{\mathbf{p}} \zeta_{\mathbf{q}} \\ &\quad + f^\zeta(\mathbf{k}, t) \\ \dot{b}_{\mathbf{k}} + (\kappa_x k_x^2 + \kappa_z k_z^2) b_{\mathbf{k}} + i k_x \zeta_{\mathbf{k}} k^{-2} &= \epsilon (2\pi)^{-2} \int_{-\infty}^{\infty} d^2 \mathbf{p} d^2 \mathbf{q} \delta(\mathbf{p} + \mathbf{q} - \mathbf{k}) (p_x q_z - p_z q_x) p^{-2} \zeta_{\mathbf{p}} b_{\mathbf{q}} \\ &\quad + f^b(\mathbf{k}, t).\end{aligned}\tag{C-9}$$

Here, $f^{b(\zeta)}(\mathbf{k}, t)$ is the Fourier transform of the forcing term of the buoyancy (vorticity), respectively. Next we define a new variable (e.g., Carnevale, 1981), $A_{s, \mathbf{k}}$, which is a wave amplitude,

$$A_{s, \mathbf{k}} = \frac{1}{2} (\zeta_{\mathbf{k}} / k + s b_{\mathbf{k}}),$$

where $s = \pm 1$ represents right and left-propagating waves. The equation of motion for the wave amplitude in the spectral domain takes the form,

$$\dot{A}_{a,\mathbf{k}} + \mathbf{L}_{ab}(\mathbf{k})A_{b,\mathbf{k}} = \epsilon \sum_{\mathbf{p},\mathbf{q}} \sum_{b,c} \delta(\mathbf{k} - \mathbf{p} - \mathbf{q}) \mathbf{M}_{abc}(\mathbf{k}, \mathbf{p}, \mathbf{q}) A_{b,\mathbf{p}} A_{c,\mathbf{q}} + F_a(\mathbf{k}), \quad (\text{C-10})$$

where the interaction coefficient $\mathbf{M}_{\pm ab}$ and the linear operator \mathbf{L}_{ab} are

$$\begin{aligned} \mathbf{M}_{\pm}(\mathbf{k}, \mathbf{p}, \mathbf{q}) &= \frac{p_x q_z - p_z q_x}{k p q} \begin{pmatrix} q^2 - p^2 \pm k(q - p) & q^2 - p^2 \mp k(q + p) \\ q^2 - p^2 \pm k(q + p) & q^2 - p^2 \mp k(q - p) \end{pmatrix} \\ \mathbf{L}(\mathbf{k}) &= \begin{pmatrix} \frac{1}{2}(\nu_x + \kappa_x)k_x^2 + \frac{1}{2}(\nu_z + \kappa_z)k_z^2 - i\frac{k_x}{k} & \frac{1}{2}(\nu_x - \kappa_x)k_x^2 + \frac{1}{2}(\nu_z - \kappa_z)k_z^2 \\ \frac{1}{2}(\nu_x - \kappa_x)k_x^2 + \frac{1}{2}(\nu_z - \kappa_z)k_z^2 & \frac{1}{2}(\nu_x + \kappa_x)k_x^2 + \frac{1}{2}(\nu_z + \kappa_z)k_z^2 + i\frac{k_x}{k} \end{pmatrix}. \end{aligned} \quad (\text{C-11})$$

The forcing term $F_s(\mathbf{k}, t) = \frac{1}{2}(f^\zeta(\mathbf{k}, t)/k + s f^b(\mathbf{k}, t))$ in the amplitude equation (C-10) is a linear combination of the forcing terms appearing on equations (C-9). The energy equation in terms of the wave amplitudes is

$$\begin{aligned} \frac{\partial}{\partial t} (A_{a,\mathbf{k}} A_{a,\mathbf{k}}^*) &= -2\text{Re} \left(\sum_b L_{ab} A_{b,\mathbf{k}} A_{a,\mathbf{k}}^* \right) + 2\text{Re} (F_a^*(\mathbf{k}) A_{a,\mathbf{k}}) \\ &+ \epsilon 2\text{Re} \left(\frac{1}{4(2\pi)^2} \int_{-\infty}^{\infty} d^2 \mathbf{q} d^2 \mathbf{p} \delta(\mathbf{k} - \mathbf{p} - \mathbf{q}) \sum_{b,c} \mathbf{M}_{abc}(\mathbf{k}, \mathbf{p}, \mathbf{q}) A_{b,\mathbf{p}} A_{c,\mathbf{q}} A_{a,\mathbf{k}}^* \right). \end{aligned} \quad (\text{C-12})$$

We next define slow amplitudes as

$$\hat{A}_{a,\mathbf{k}} = A_{a,\mathbf{k}} e^{-i a \omega_{\mathbf{k}} t}. \quad (\text{C-13})$$

To simplify the RHS of equation (C-12), we need an equation of motion for the third moment, which, after neglecting molecular viscosity and diffusion, is

$$\left(\hat{A}_{a,\mathbf{k}}^* \hat{A}_{b,\mathbf{p}} \hat{A}_{c,\mathbf{q}} \right)_t = e^{i \Delta \omega(\mathbf{k}, \mathbf{p}, \mathbf{q}, a, b, c) t} \epsilon \mathcal{N}_{abc}(\mathbf{k}, \mathbf{p}, \mathbf{q}). \quad (\text{C-14})$$

where $\Delta \omega(\mathbf{k}, \mathbf{p}, \mathbf{q}, a, b, c) \equiv (a \omega_{\mathbf{k}} - b \omega_{\mathbf{p}} - c \omega_{\mathbf{q}})$ and $\mathcal{N}_{abc}(\mathbf{k}, \mathbf{p}, \mathbf{q})$ on the RHS is given by

$$\begin{aligned} \mathcal{N}_{abc}(\mathbf{k}, \mathbf{p}, \mathbf{q}) &= \frac{1}{4(2\pi)^2} \int_{-\infty}^{\infty} d^2 \mathbf{n} d^2 \mathbf{r} \delta(\mathbf{k} - \mathbf{r} - \mathbf{n}) \mathbf{M}_{adf}^*(\mathbf{k}, \mathbf{r}, \mathbf{n}) A_{d,\mathbf{r}}^* A_{f,\mathbf{n}}^* A_{b,\mathbf{p}} A_{c,\mathbf{q}} \\ &+ \frac{1}{4(2\pi)^2} \int_{-\infty}^{\infty} d^2 \mathbf{n} d^2 \mathbf{r} \delta(\mathbf{p} - \mathbf{r} - \mathbf{n}) \mathbf{M}_{bdf}(\mathbf{p}, \mathbf{r}, \mathbf{n}) A_{a,\mathbf{k}}^* A_{c,\mathbf{q}} A_{d,\mathbf{r}} A_{f,\mathbf{n}} \\ &+ \frac{1}{4(2\pi)^2} \int_{-\infty}^{\infty} d^2 \mathbf{n} d^2 \mathbf{r} \delta(\mathbf{q} - \mathbf{r} - \mathbf{n}) \mathbf{M}_{cdf}(\mathbf{q}, \mathbf{r}, \mathbf{n}) A_{a,\mathbf{k}}^* A_{b,\mathbf{p}} A_{d,\mathbf{r}} A_{f,\mathbf{n}}. \end{aligned} \quad (\text{C-15})$$

In the common derivation of the kinetic equation, at this stage, an ensemble average is taken over both sides of equation (C-14), and one makes use of assumptions of spatial homogeneity (translation invariance),

$$\langle A_{a,\mathbf{p}} A_{b,\mathbf{q}} \rangle = 2(2\pi)^2 \delta(\mathbf{p} + \mathbf{q}) \Phi_{ab}(\mathbf{p}). \quad (\text{C-16})$$

Further, assuming that right and left-propagating waves do not interact allows us to write

$$\langle A_{a,\mathbf{p}} A_{b,\mathbf{q}} \rangle = 2(2\pi)^2 \delta(\mathbf{p} + \mathbf{q}) \delta_{a,b} \Phi_{aa}(\mathbf{p}). \quad (\text{C-17})$$

The final stage in the derivation of the kinetic equation is to use the Gaussian approximation in order to replace the fourth-order moment with products of second-order moments.

D First derivation: a two timescale perturbative approach

In the first derivation considered here of the resonant condition on the frequencies of interacting waves, one uses a multiple timescale perturbative approach (see Benney and Saffman (1966), or as outlined in the context of internal waves in, e.g., Caillol and Zeitlin (2000), with the general multiple timescale perturbative method described in section 11.2 of Bender and Orszag (1978)). We start by assuming that the solution can be expanded in the small parameter, ϵ , namely,

$$A_{s,\mathbf{k}} = A_{s,\mathbf{k},0} + \epsilon A_{s,\mathbf{k},1} + \epsilon^2 A_{s,\mathbf{k},2} + \dots = \sum_{m=0}^{\infty} \epsilon^m A_{s,\mathbf{k},m}. \quad (\text{D-18})$$

We also assume a timescale separation, namely, we define a slow time $\tau = \epsilon t$ and the full time derivative is assumed to be of the form $\frac{d}{dt} = \frac{\partial}{\partial t} + \epsilon \frac{\partial}{\partial \tau}$. By substituting the expansion above in the amplitude equation (eq. (2) in the main text), it takes the following form

$$\begin{aligned} & \frac{\partial}{\partial t} \sum_{m=0}^{\infty} \epsilon^m A_{s,\mathbf{k},m} + \frac{\partial}{\partial \tau} \sum_{m=0}^{\infty} \epsilon^{m+1} A_{s,\mathbf{k},m} + L_{sr} \sum_{m=0}^{\infty} \epsilon^m A_{r,\mathbf{k},m} \\ &= \frac{\epsilon}{4(2\pi)^2} \int_{-\infty}^{\infty} d^2 \mathbf{q} d^2 \mathbf{p} \delta(\mathbf{k} - \mathbf{p} - \mathbf{q}) M_{sab}(\mathbf{k}, \mathbf{p}, \mathbf{q}) \sum_{m=0}^{\infty} \epsilon^m A_{a,\mathbf{p},m} \sum_{m'=0}^{\infty} \epsilon^{m'} A_{b,\mathbf{q},m'} + F_s(\mathbf{k}). \end{aligned} \quad (\text{D-19})$$

The zeroth order variable simply satisfies the linear equation,

$$\frac{\partial}{\partial t} A_{s,\mathbf{k},0} + L_{sr} A_{r,\mathbf{k},0} = F_s(\mathbf{k}), \quad (\text{D-20})$$

with a solution for \mathbf{k} away from the forced wavenumbers of the form (neglecting dissipation and diffusion),

$$A_{s,\mathbf{k},0} = \hat{A}_{s,\mathbf{k}}(\tau) e^{is\omega(\mathbf{k})t}. \quad (\text{D-21})$$

The equation for the first order is

$$\frac{\partial}{\partial t} A_{s,\mathbf{k},1} + L_{sr} A_{r,\mathbf{k},1} = -\frac{\partial}{\partial \tau} A_{s,\mathbf{k},0} + \frac{1}{4(2\pi)^2} \int_{-\infty}^{\infty} d^2 \mathbf{q} d^2 \mathbf{p} \delta(\mathbf{k} - \mathbf{p} - \mathbf{q}) M_{sab}(\mathbf{k}, \mathbf{p}, \mathbf{q}) A_{a,\mathbf{p},0} A_{b,\mathbf{q},0}. \quad (\text{D-22})$$

Substituting the solution of the zeroth order, the RHS becomes

$$e^{is\omega(\mathbf{k})t} \left(-\frac{\partial}{\partial \tau} \hat{A}_{s,\mathbf{k}}(\tau) + \frac{1}{4(2\pi)^2} \int_{-\infty}^{\infty} d^2 \mathbf{q} d^2 \mathbf{p} \delta(\mathbf{k} - \mathbf{p} - \mathbf{q}) M_{sab}(\mathbf{k}, \mathbf{p}, \mathbf{q}) \hat{A}_{a,\mathbf{p}}(\tau) \hat{A}_{b,\mathbf{q}}(\tau) e^{-i\Delta\omega(\mathbf{k},\mathbf{p},\mathbf{q},s,a,b)t} \right), \quad (\text{D-23})$$

This is proportional to $e^{is\omega(\mathbf{k})t}$, which is the solution to the LHS operator and, thus, may result in a secular term that grows linearly in t and invalidates the perturbation expansion for large t . In order to prevent a secular term in the solution for the first-order variables, we demand that the expression in the parentheses, which is the coefficient of the term that leads to a secular term, vanishes. Because the first term in the parentheses is only a function of τ , this implies that the second term, the integral, should not be a function of t as well. The only way to satisfy this condition is that the integrand is negligible unless

$$\Delta\omega(\mathbf{k}, \mathbf{p}, \mathbf{q}, s, a, b) = s\omega(\mathbf{k}) - a\omega(\mathbf{p}) - b\omega(\mathbf{q}) = 0, \quad (\text{D-24})$$

In other words, the consistency condition is

$$\delta(\mathbf{k} - \mathbf{p} - \mathbf{q}) M_{sab}(\mathbf{k}, \mathbf{p}, \mathbf{q}) \hat{A}_{a,\mathbf{p}}(\tau) \hat{A}_{b,\mathbf{q}}(\tau) \propto \delta(\Delta\omega(\mathbf{k}, \mathbf{p}, \mathbf{q}, s, a, b)), \quad (\text{D-25})$$

namely, the resonance condition, which needs to be satisfied for any (slow) time τ . This implies that the amplitude $\hat{A}_{b,\mathbf{p}}(\tau)$ must be small for \mathbf{p} away from the resonance, and large for \mathbf{p} in which the resonance condition is satisfied. However, as pointed out in the paper itself, for different \mathbf{k} values, a specific \mathbf{p} value might be in the resonance for one \mathbf{k} and out of resonance for the other. It is, therefore, not clear how this condition can be satisfied for all \mathbf{k} values simultaneously.

E Second derivation: assuming a slowly varying triple correlation

The derivation of the kinetic equation involves a slow amplitude assumption and a Gaussian decomposition of a fourth-order correlation. The two approximations are independent and can be done in several ways. Consider taking the slow amplitude assumption first. Neglecting the viscosity and diffusion, the time-averaged energy equation (C-12) in terms of the slow wave amplitudes becomes

$$\begin{aligned} \frac{1}{T} \int_0^T \frac{\partial}{\partial t} (A_{a,\mathbf{k}} A_{a,\mathbf{k}}^*) dt &= 2Re \left(\frac{1}{4(2\pi)^2} \int_{-\infty}^{\infty} d^2\mathbf{q} d^2\mathbf{p} \delta(\mathbf{k} - \mathbf{p} - \mathbf{q}) \sum_{b,c} M_{abc}(\mathbf{k}, \mathbf{p}, \mathbf{q}) \right. \\ &\times \left. \frac{1}{T} \int_0^T \hat{A}_{b,\mathbf{p}} \hat{A}_{c,\mathbf{q}} \hat{A}_{a,\mathbf{k}}^* e^{-i\Delta\omega(\mathbf{k}, \mathbf{p}, \mathbf{q}, a, b, c)t} dt \right) + 2Re \left(\frac{1}{T} \int_0^T F_a^*(\mathbf{k}) e^{i\omega_{\mathbf{k}}t} \hat{A}_{a,\mathbf{k}} dt \right). \end{aligned} \quad (\text{E-26})$$

The RHS involves the following integral,

$$Y \equiv Re \left(\frac{1}{T} \int_0^T \hat{A}_{b,\mathbf{p}} \hat{A}_{c,\mathbf{q}} \hat{A}_{a,\mathbf{k}}^* e^{-i\Delta\omega(\mathbf{k}, \mathbf{p}, \mathbf{q}, a, b, c)t} dt \right). \quad (\text{E-27})$$

If one assumes that the amplitudes do not vary significantly over the averaging period, T , X may be estimated by

$$X \equiv Re \left(\frac{1}{T} \int_0^T \hat{A}_{b,\mathbf{p}} \hat{A}_{c,\mathbf{q}} \hat{A}_{a,\mathbf{k}}^* dt \times \frac{1}{T} \int_0^T e^{-i\Delta\omega(\mathbf{k}, \mathbf{p}, \mathbf{q}, a, b, c)t} dt \right). \quad (\text{E-28})$$

The normalized difference between X and Y (V_2 , equation (10) in the main text) is used in the paper as a measure of the validity of the slow amplitude assumption. Under the slow amplitude assumption, $\hat{A}_{s,\mathbf{k}}$ is not a function of t , and the integral in X may be written as

$$\begin{aligned} X &\approx Re \left(\hat{A}_{b,\mathbf{p}} \hat{A}_{c,\mathbf{q}} \hat{A}_{a,\mathbf{k}}^* \frac{1}{T} \int_0^T e^{-i\Delta\omega(\mathbf{k}, \mathbf{p}, \mathbf{q}, a, b, c)t} dt \right) \\ &= Re \left(\hat{A}_{b,\mathbf{p}} \hat{A}_{c,\mathbf{q}} \hat{A}_{a,\mathbf{k}}^* \delta_T(\Delta\omega(\mathbf{k}, \mathbf{p}, \mathbf{q}, a, b, c)) \right), \end{aligned} \quad (\text{E-29})$$

where

$$\delta_T \equiv \frac{1}{T} \frac{e^{-i\Delta\omega(\mathbf{k}, \mathbf{p}, \mathbf{q}, a, b, c)T} - 1}{-i\Delta\omega(\mathbf{k}, \mathbf{p}, \mathbf{q}, a, b, c)}. \quad (\text{E-30})$$

In the limit of $T \rightarrow \infty$, we have

$$\begin{aligned} \lim_{T \rightarrow \infty} \text{Re}(\delta_T(\Delta\omega(\mathbf{k}, \mathbf{p}, \mathbf{q}, a, b, c))) &= \lim_{T \rightarrow \infty} \frac{\sin(\Delta\omega(\mathbf{k}, \mathbf{p}, \mathbf{q}, a, b, c)T)}{\Delta\omega(\mathbf{k}, \mathbf{p}, \mathbf{q}, a, b, c)T} \\ &= \delta(\Delta\omega(\mathbf{k}, \mathbf{p}, \mathbf{q}, a, b, c)) \end{aligned} \quad (\text{E-31})$$

and the product of three slow amplitudes is multiplied by a Dirac delta function of $\Delta\omega$, namely, we obtain the resonance condition on the frequencies of the interacting waves in (E-26).

F Third derivation: simplifying the fourth moment using an ensemble average and Gaussian approximation

In this derivation of the constraint on the frequencies of interacting waves, we write the formal solution of the equation for the triple product, equation (C-14), and apply an ensemble average,

$$\left\langle \hat{A}_{a,\mathbf{k}}^* \hat{A}_{b,\mathbf{p}} \hat{A}_{c,\mathbf{q}} \right\rangle \Big|_0^t = \epsilon \int_0^t e^{-i\Delta\omega(\mathbf{k}, \mathbf{p}, \mathbf{q}, a, b, c)t'} \langle \mathcal{N}_{abc}(\mathbf{k}, \mathbf{p}, \mathbf{q}) \rangle dt'. \quad (\text{F-32})$$

At this stage, one makes use of the assumption of spatial homogeneity (translation invariance, (C-16)), and further assumes that right and left-propagating waves do not interact (are not correlated, (C-17)). Finally, one uses the Gaussian decomposition of the four-point correlation,

$$\begin{aligned} \langle \hat{A}_{a,\mathbf{r}} \hat{A}_{b,\mathbf{n}} \hat{A}_{c,\mathbf{p}} \hat{A}_{d,\mathbf{q}} \rangle &= \langle \hat{A}_{a,\mathbf{r}} \hat{A}_{b,\mathbf{n}} \rangle \langle \hat{A}_{c,\mathbf{p}} \hat{A}_{d,\mathbf{q}} \rangle \\ &+ \langle \hat{A}_{a,\mathbf{r}} \hat{A}_{c,\mathbf{p}} \rangle \langle \hat{A}_{b,\mathbf{n}} \hat{A}_{d,\mathbf{q}} \rangle + \langle \hat{A}_{a,\mathbf{r}} \hat{A}_{d,\mathbf{q}} \rangle \langle \hat{A}_{b,\mathbf{n}} \hat{A}_{c,\mathbf{p}} \rangle. \end{aligned} \quad (\text{F-33})$$

Together, these approximations and assumptions lead to the following simplification of the nonlinear interaction term in the energy equation,

$$\begin{aligned}
\langle \mathcal{N}_{abc}(\mathbf{k}, \mathbf{p}, \mathbf{q}) \rangle &= (2\pi)^2 \int_{-\infty}^{\infty} d^2\mathbf{n} d^2\mathbf{r} \delta(\mathbf{k} - \mathbf{r} - \mathbf{n}) M_{adf}^*(\mathbf{k}, \mathbf{r}, \mathbf{n}) \\
&\quad \left(\delta(\mathbf{r} + \mathbf{n}) \delta(\mathbf{p} + \mathbf{q}) \delta_{b,c} \delta_{d,f} \Phi_{dd}(\mathbf{r}) \Phi_{bb}(\mathbf{p}) \right. \\
&\quad + \delta(\mathbf{q} - \mathbf{n}) \delta(\mathbf{p} - \mathbf{r}) \delta_{d,b} \delta_{c,f} \Phi_{bb}(\mathbf{p}) \Phi_{cc}(\mathbf{q}) \\
&\quad \left. + \delta(\mathbf{q} - \mathbf{n}) \delta(\mathbf{p} - \mathbf{r}) \delta_{f,c} \delta_{d,b} \Phi_{dd}(\mathbf{r}) \Phi_{bb}(\mathbf{p}) \right) \\
&\quad + (2\pi)^2 \int_{-\infty}^{\infty} d^2\mathbf{n} d^2\mathbf{r} \delta(\mathbf{p} - \mathbf{r} - \mathbf{n}) M_{bdf}(\mathbf{p}, \mathbf{r}, \mathbf{n}) \Phi_{aa}(\mathbf{k}) \\
&\quad \left(\delta(\mathbf{k} - \mathbf{q}) \delta_{a,c} \delta(\mathbf{r} + \mathbf{n}) \delta_{d,f} \Phi_{dd}(\mathbf{r}) \right. \\
&\quad + \delta(\mathbf{k} - \mathbf{r}) \delta_{a,d} \delta(\mathbf{q} + \mathbf{n}) \delta_{c,f} \Phi_{cc}(\mathbf{q}) \\
&\quad \left. + \delta(\mathbf{k} - \mathbf{n}) \delta_{a,f} \delta(\mathbf{r} + \mathbf{q}) \delta_{d,c} \Phi_{dd}(\mathbf{r}) \right) \\
&\quad + (2\pi)^2 \int_{-\infty}^{\infty} d^2\mathbf{n} d^2\mathbf{r} \delta(\mathbf{q} - \mathbf{r} - \mathbf{n}) M_{cdf}(\mathbf{q}, \mathbf{r}, \mathbf{n}) \Phi_{aa}(\mathbf{k}) \\
&\quad \left(\delta(\mathbf{k} - \mathbf{p}) \delta_{a,b} \delta(\mathbf{r} + \mathbf{n}) \delta_{d,f} \Phi_{dd}(\mathbf{r}) \right. \\
&\quad + \delta(\mathbf{k} - \mathbf{r}) \delta_{a,d} \delta(\mathbf{p} + \mathbf{n}) \delta_{b,f} \Phi_{bb}(\mathbf{p}) \\
&\quad \left. + \delta(\mathbf{k} - \mathbf{n}) \delta_{a,f} \delta(\mathbf{p} + \mathbf{r}) \delta_{b,d} \Phi_{bb}(\mathbf{p}) \right). \tag{F-34}
\end{aligned}$$

where $\Phi_{ab}(\mathbf{k}) = \langle \hat{A}_{a,\mathbf{k}} \hat{A}_{b,\mathbf{k}} \rangle$. Taking into account the fact that $M_{abc}(\mathbf{k}, \mathbf{r}, \mathbf{r}) = M_{abc}(\mathbf{k}, \mathbf{r}, -\mathbf{r}) = 0$ and the fact that $M_{abc}(\mathbf{k}, \mathbf{p}, \mathbf{q})$ is real, and $M_{abc}(\mathbf{k}, \mathbf{p}, \mathbf{q}) = M_{acb}(\mathbf{k}, \mathbf{q}, \mathbf{p})$, the expression above may be simplified to:

$$\begin{aligned}
\langle \mathcal{N}_{abc}(\mathbf{k}, \mathbf{p}, \mathbf{q}) \rangle &= 2(2\pi)^2 \delta(\mathbf{k} - \mathbf{p} - \mathbf{q}) \\
&\quad \left[M_{abc}(\mathbf{k}, \mathbf{p}, \mathbf{q}) \Phi_{bb}(\mathbf{p}) \Phi_{cc}(\mathbf{q}) - M_{bac}(\mathbf{p}, \mathbf{k}, \mathbf{q}) \Phi_{aa}(\mathbf{k}) \Phi_{cc}(\mathbf{q}) - M_{cab}(\mathbf{q}, \mathbf{k}, \mathbf{p}) \Phi_{aa}(\mathbf{k}) \Phi_{bb}(\mathbf{p}) \right] \tag{F-35}
\end{aligned}$$

Substituting the solution for the third-order correlation function, in terms of the fourth-order correlation function, into the energy equation (C-12), and defining $E_{a,\mathbf{k}}(t) = \langle A_{a,\mathbf{k}}^* A_{a,\mathbf{k}} \rangle / V = \frac{1}{2} \langle (u_{\mathbf{k}}^2 + w_{\mathbf{k}}^2 + b_{\mathbf{k}}^2) \rangle / V$ where V is the domain volume, results in the kinetic equation for the energy spectrum. In terms of the two-point correlation function, $E_{a,\mathbf{k}} = 2(2\pi)^2 \Phi_{aa}(\mathbf{k})$. Using these definitions, the equation for the energy

spectrum may be written as,

$$\begin{aligned}
\frac{\partial}{\partial t} E_a(\mathbf{k}, t) = & \frac{1}{4(2\pi)^4} \text{Re} \left(\int_{-\infty}^{\infty} d^2\mathbf{q} d^2\mathbf{p} \delta(\mathbf{k} - \mathbf{p} - \mathbf{q}) \sum_{b,c} M_{abc}(\mathbf{k}, \mathbf{p}, \mathbf{q}) \right. \\
& \int_0^t dt' e^{-i\Delta\omega(\mathbf{k}, \mathbf{p}, \mathbf{q}, a, b, c)(t-t')} \left[M_{abc}(\mathbf{k}, \mathbf{p}, \mathbf{q}) E_b(\mathbf{p}, t') E_c(\mathbf{q}, t') \right. \\
& \left. - M_{bac}(\mathbf{p}, \mathbf{k}, \mathbf{q}) E_a(\mathbf{k}, t') E_c(\mathbf{q}, t') - M_{cab}(\mathbf{q}, \mathbf{k}, \mathbf{p}) E_a(\mathbf{k}, t') E_b(\mathbf{p}, t') \right] \Bigg) \\
& + 2\text{Re}(\langle F_a^*(\mathbf{k}) A_{a,\mathbf{k}} \rangle). \tag{F-36}
\end{aligned}$$

One may write the integral over time that appears on the RHS of the above energy equation as

$$\int_0^t dt' e^{-i(a\omega_{\mathbf{k}} - b\omega_{\mathbf{p}} - c\omega_{\mathbf{q}})(t-t')} \mathcal{G}(\langle E(t') \rangle) dt', \tag{F-37}$$

where

$$\begin{aligned}
\mathcal{G}(\langle E(t') \rangle) = & \left[M_{abc}(\mathbf{k}, \mathbf{p}, \mathbf{q}) E_b(\mathbf{p}, t') E_c(\mathbf{q}, t') \right. \\
& \left. - M_{bac}(\mathbf{p}, \mathbf{k}, \mathbf{q}) E_a(\mathbf{k}, t') E_c(\mathbf{q}, t') - M_{cab}(\mathbf{q}, \mathbf{k}, \mathbf{p}) E_a(\mathbf{k}, t') E_b(\mathbf{p}, t') \right]. \tag{F-38}
\end{aligned}$$

The final steps of assuming that the ensemble-averaged energy spectrum varies slowly in time, taking the limit $t \rightarrow \infty$, and taking the slowly varying ensemble-averaged energies out of the time integral, lead to the resonant interaction constraint on the frequencies of interacting waves,

$$\begin{aligned}
& \int_0^t e^{-i(a\omega_{\mathbf{k}} - b\omega_{\mathbf{p}} - c\omega_{\mathbf{q}})(t-t')} dt' \frac{1}{t} \int_0^t \mathcal{G}(\langle E(t'') \rangle) dt'' \\
& = \delta(a\omega_{\mathbf{k}} - b\omega_{\mathbf{p}} - c\omega_{\mathbf{q}}) 2\pi \int_0^t \mathcal{G}(\langle E(t'') \rangle) dt''. \tag{F-39}
\end{aligned}$$

The consistency of this derivation, in particular the requirement that $\mathcal{G}(\langle E(t'') \rangle)$ is slowly varying relative to the oscillating term, can be quantified by the conditions represented by equations (11) and (13) (in the main text). These quantities are analyzed in the main text for testing the consistency of the RWIA.

G Supplementary figures

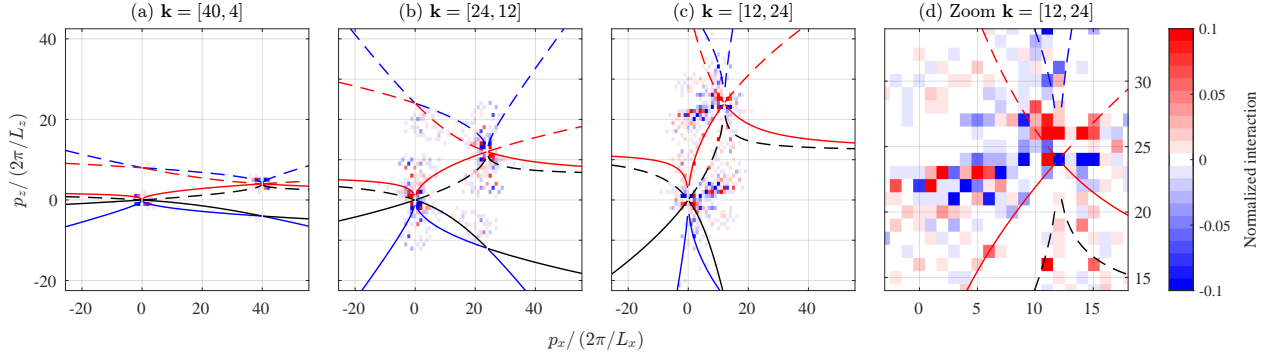


Figure G.1: (a–c) Time-average of the interaction term (the expression in blue on the second line of eq. (3) in the main text) for $\mathbf{k} = (40, 4)$, $(24, 12)$, and $(12, 24)$, for the **weakly forced** run, normalized (for each \mathbf{k}) by its maximum value, **zooming in the contour range close to zero to see a wider range of interacting wavenumbers**. The color range corresponds only to about a third of the range of values plotted to highlight weaker interactions. (d) A zoom into the region of $\mathbf{p} \sim \mathbf{k}$ for panel (c). The lines represent the resonance curves.

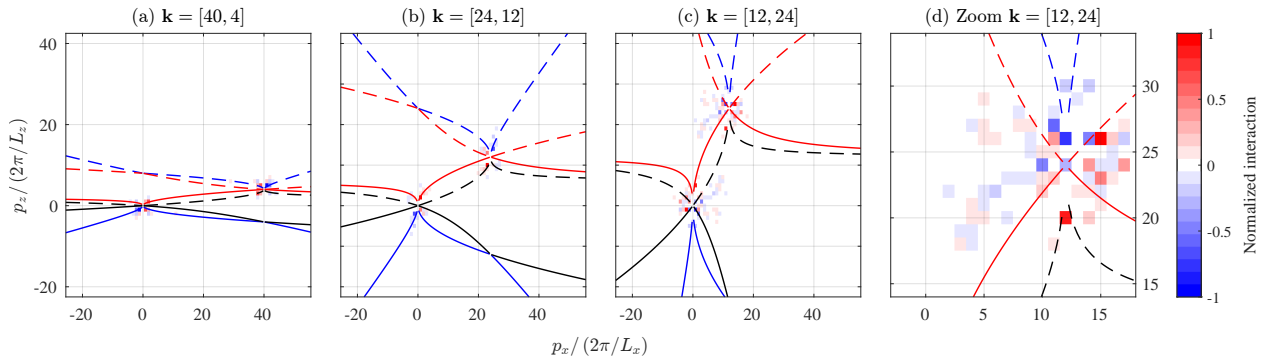


Figure G.2: (a–c) Time-average of the interaction term (the expression in blue on the second line of eq. (3) in the main text) for $\mathbf{k} = (40, 4)$, $(24, 12)$, and $(12, 24)$, for the **medium forced** run, normalized (for each \mathbf{k}) by its maximum value. The color range corresponds only to about a third of the range of values plotted to highlight weaker interactions. (d) A zoom into the region of $\mathbf{p} \sim \mathbf{k}$ for panel (c). The lines represent the resonance curves.

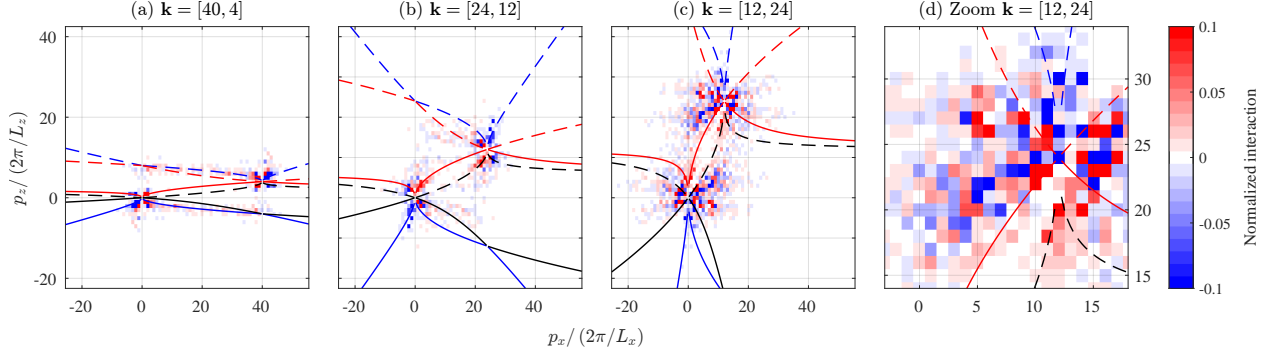


Figure G.3: (a–c) Time-average of the interaction term (the expression in blue on the second line of eq. (3) in the main text) for $\mathbf{k} = (40, 4)$, $(24, 12)$, and $(12, 24)$, for the **medium forced** run, normalized (for each \mathbf{k}) by its maximum value, **zooming in the contour range close to zero to see a wider range of interacting wavenumbers**. The color range corresponds only to about a third of the range of values plotted to highlight weaker interactions. (d) A zoom into the region of $\mathbf{p} \sim \mathbf{k}$ for panel (c). The lines represent the resonance curves.

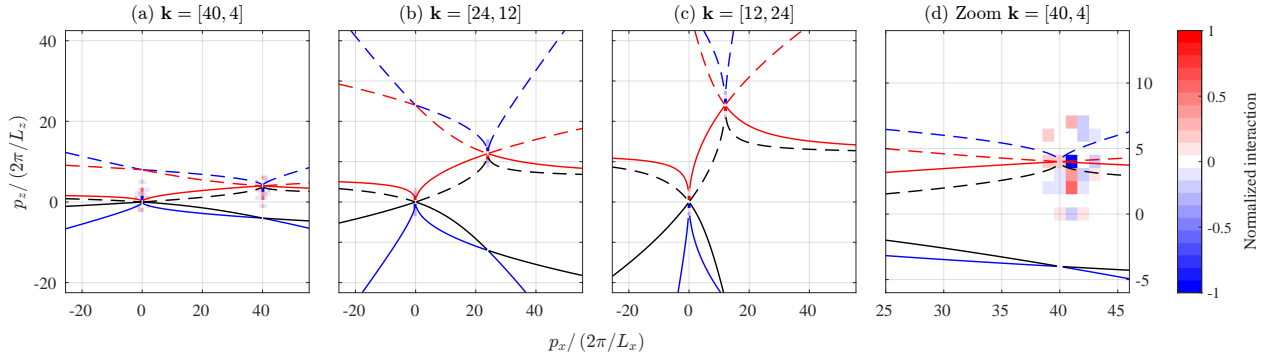


Figure G.4: (a–c) Time-average of the interaction term (the expression in blue on the second line of eq. (3)) for $\mathbf{k} = (40, 4)$, $(24, 12)$, and $(12, 24)$, for the **strongly forced** run, normalized (for each \mathbf{k}) by its maximum value. The color range corresponds only to about a third of the range of values plotted, to highlight weaker interactions. (d) A zoom into the region of $\mathbf{p} \sim \mathbf{k}$ for panel (c). The lines represent the resonance curves.

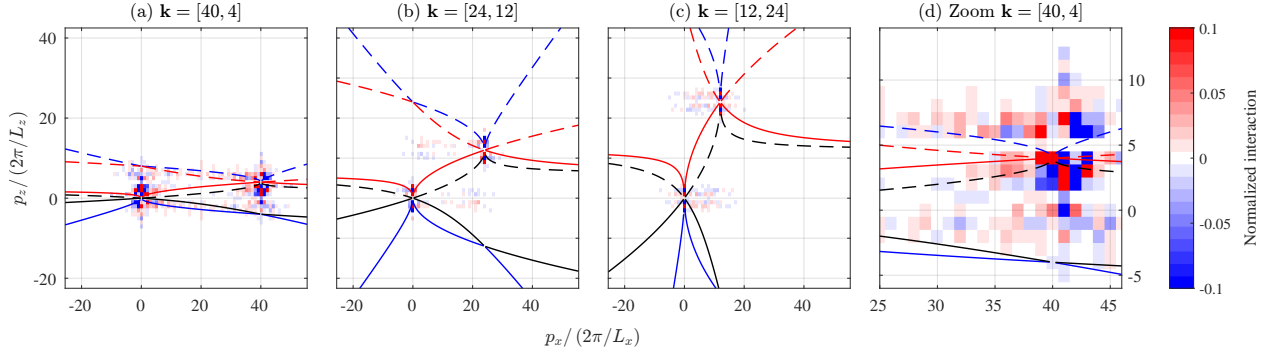


Figure G.5: (a–c) Time-average of the interaction term (the expression in blue on the second line of eq. (3)) for $\mathbf{k} = (40, 4)$, $(24, 12)$, and $(12, 24)$, for the **strongly forced** run, normalized (for each \mathbf{k}) by its maximum value, **zooming in the contour range close to zero to see a wider range of interacting wavenumbers**. The color range corresponds only to about a third of the range of values plotted, to highlight weaker interactions. (d) A zoom into the region of $\mathbf{p} \sim \mathbf{k}$ for panel (c). The lines represent the resonance curves.

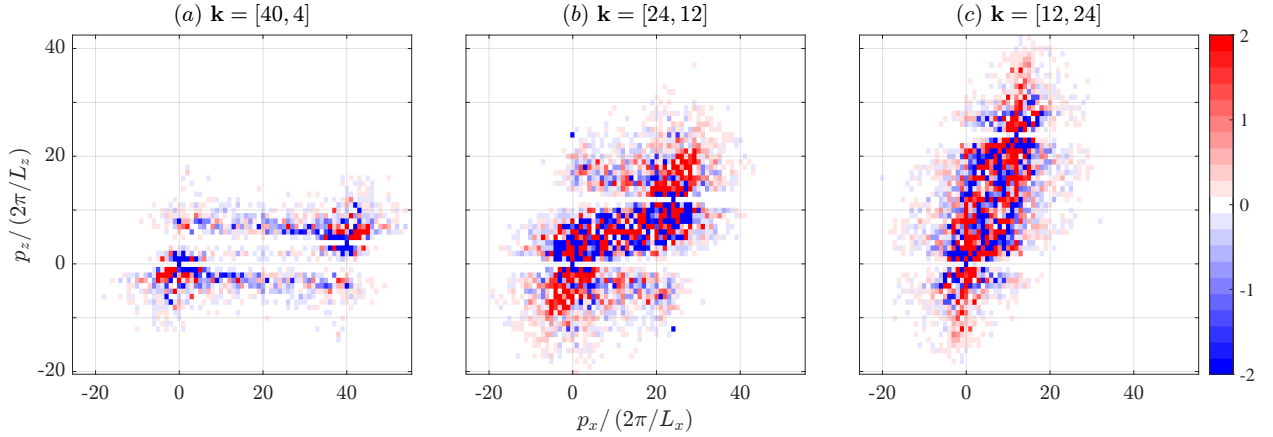


Figure G.6: Testing whether the three-product of wave amplitudes slowly varies (criterion V_2 , eq. (10) in the main text) for the medium forcing case, for the denoted wavevectors.

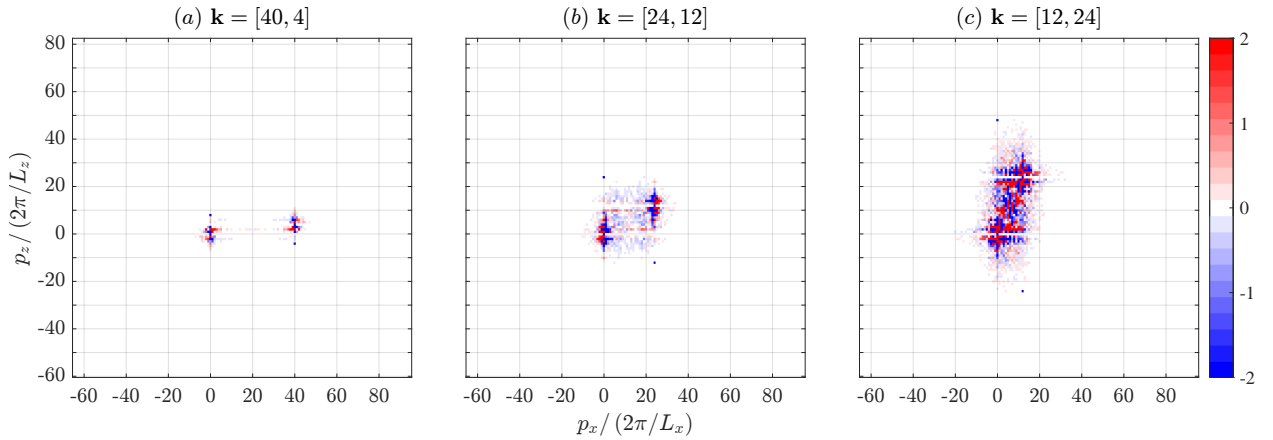


Figure G.7: Testing whether the three-product of wave amplitudes slowly varies (criterion V_2 , eq. (10) in the main text) for the strong forcing case, for the denoted wavevectors.

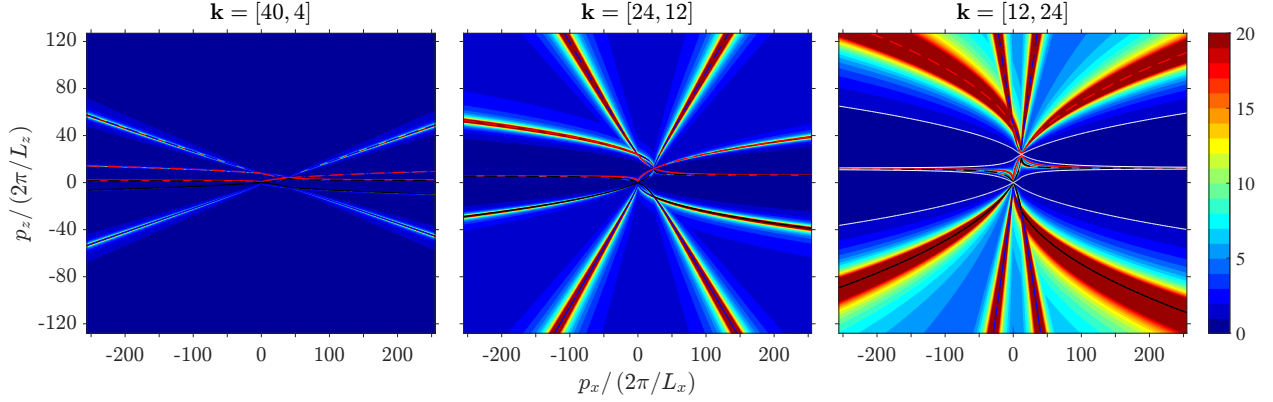


Figure G.8: The period of the oscillating term in the equation for the three-product of the slow wave amplitudes eq. (F-32), $2\pi/\Delta\omega$, in units of days (criterion V_3 , equation (11), using $T = 1$ day). On the resonant curves, this period diverges, and it is also not small in their vicinity, in contradiction to the assumption used to derive the resonant condition on the frequencies of the interacting waves. The period is shown for three wavevectors, $\mathbf{k} = (40, 4)$, $(24, 12)$, $(12, 24)$. The values shown represent the maximum of V_3 with respect to the indices a, b, c .

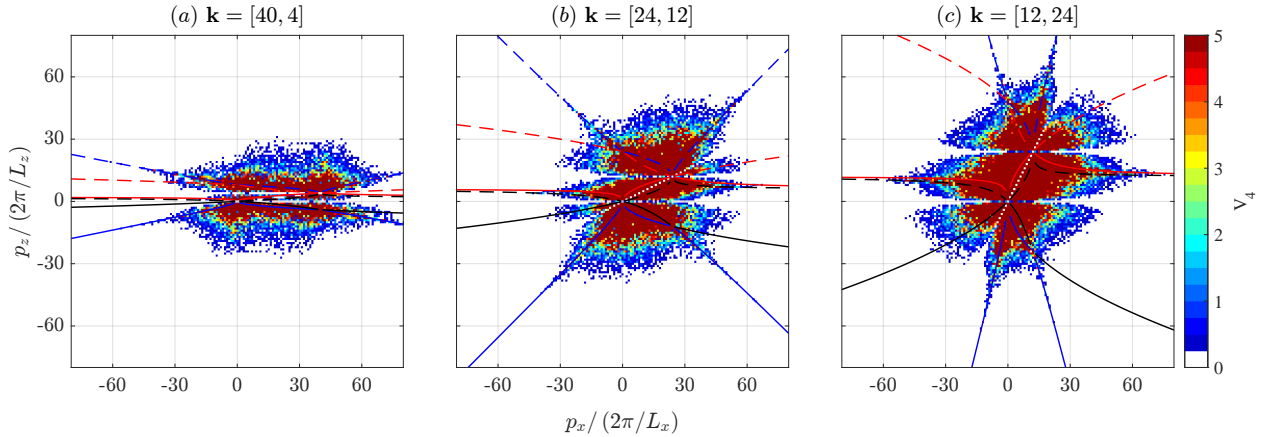


Figure G.9: The ratio between the nonlinear timescale and the wave triad timescale (V_4) of right propagating waves ($a = 1$) for the medium-forcing simulation. V_4 should be much smaller than 1 for the RWIA to be valid (see eq. (13) in the main text). The ratio is presented for three wavevectors, $\mathbf{k} = (40, 4)$, $(24, 12)$, and $(12, 24)$.

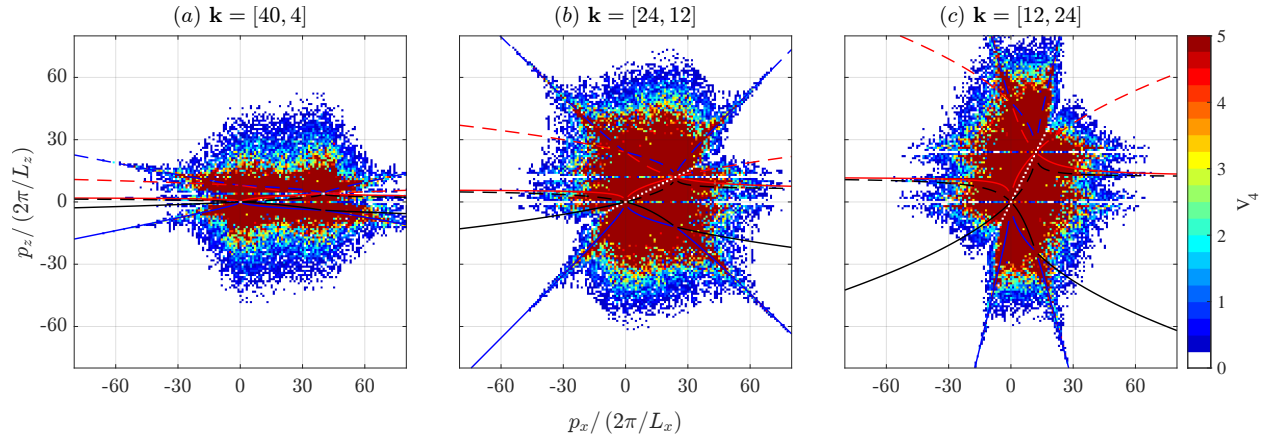


Figure G.10: The ratio between the nonlinear timescale and the wave triad timescale (V_4) of right propagating waves ($a = 1$) for the medium-forcing simulation. V_4 should be much smaller than 1 for the RWIA to be valid (see eq. (13) in the main text). The ratio is presented for three wavevectors, $\mathbf{k} = (40, 4)$, $(24, 12)$, and $(12, 24)$.